International Journal of Solids and Structures 46 (2009) 480–506

Contents lists available at ScienceDirect

International Journal of Solids and Structures

journal homepage: www.elsevier.com/locate/ijsolstr

Porous materials with two populations of voids under internal pressure: I. Instantaneous constitutive relations

Pierre-Guy Vincent [a,b], Yann Monerie [a,c], Pierre Suquet [b,*]

[a] Institut de Radioprotection et de Sûreté Nucléaire, B.P. 3, 13115 Saint-Paul-lez-Durance Cedex, France
[b] Laboratoire de Mécanique et d'Acoustique, 31 Chemin Joseph Aiguier, 13402 Marseille Cedex 20, France
[c] Laboratoire de Micromécanique et d'Intégrité des Structures, IRSN-CNRS-UMII, B.P. 3, 13115, Saint-Paul-lez-Durance Cedex, France

ARTICLE INFO

Article history:
Received 29 May 2008
Received in revised form 4 September 2008
Available online 12 September 2008

Keywords:
Damage
Plasticity
Micromechanics

ABSTRACT

This study is devoted to the mechanical behavior of uranium dioxide (UO_2) which is a porous material with two populations of voids of very different size subjected to internal pressure. The smallest voids are intragranular and spherical in shape whereas the largest pores located at the grain boundary are ellipsoidal and randomly oriented. In this first part of the study, attention is focused on the effective properties of these materials with *fixed* microstructure. In a first step, the poro-elastic properties of these doubly voided materials are studied. Then two rigorous upper bounds are derived for the effective poro-plastic constitutive relations of these materials. The first bound, obtained by generalizing the approach of Gologanu et al. (Gologanu, M., Leblond, J., Devaux, J., 1994. Approximate models for ductile metals containing non-spherical voids-case of axisymmetric oblate ellipsoidal cavities. ASME J. Eng. Mater. Technol. 116, 290–297) to compressible materials, is accurate at high stress-triaxiality. The second one, which derives from the variational method of Ponte Castañeda (Ponte Castañeda, P., 1991. The effective mechanical properties of non-linear isotropic composites. J. Mech. Phys. Solids 39, 45–71), is accurate when the stress triaxiality is low. A *N*-phase model, inspired by Bilger et al. (Bilger, N., Auslender, F., Bornert, M., Masson, R., 2002. New bounds and estimates for porous media with rigid perfectly plastic matrix. C.R. Mécanique 330, 127–132), is proposed which matches the best of the two bounds at low and high triaxiality. The effect of internal pressures is discussed. In particular it is shown that when the two internal pressures coincide, the effective flow surface of the saturated biporous material is obtained from that of the drained material by a shift along the hydrostatic axis. However, when the two pressures are different, the modifications brought to the effective flow surface in the drained case involve not only a shift along the hydrostatic axis but also a change in shape and size of the surface.

1. Introduction

This study is devoted to the mechanical behavior of uranium dioxide (UO_2) to assess the safety of nuclear fuel rods under accident conditions. UO_2 is a polycrystalline material with grain size of about 10 μm, depending on the compaction process at fabrication and on the burn-up (irradiation level) (Olander, 1976; Dherbey et al., 2002; Kashibe and Une, 1991). When highly irradiated, its microstructure shows two populations of cavities of rather different sizes and shapes (Fig. 1). At the smallest scale (microscopic scale), a first population of cavities, almost spherical in shape with a typical diameter of a few nanometers can be found in the interior of the grains (they are referred to as *intragranular voids*). At a larger scale (meso-

* Corresponding author. Tel.: +334 91 16 42 08; fax: +33 4 91 16 44 81.
E-mail addresses: pierre-guy.vincent@irsn.fr (P.-G. Vincent), yann.monerie@irsn.fr (Y. Monerie), suquet@lma.cnrs-mrs.fr (P. Suquet).

0020-7683/$ - see front matter © 2008 Elsevier Ltd. All rights reserved.
doi:10.1016/j.ijsolstr.2008.09.003

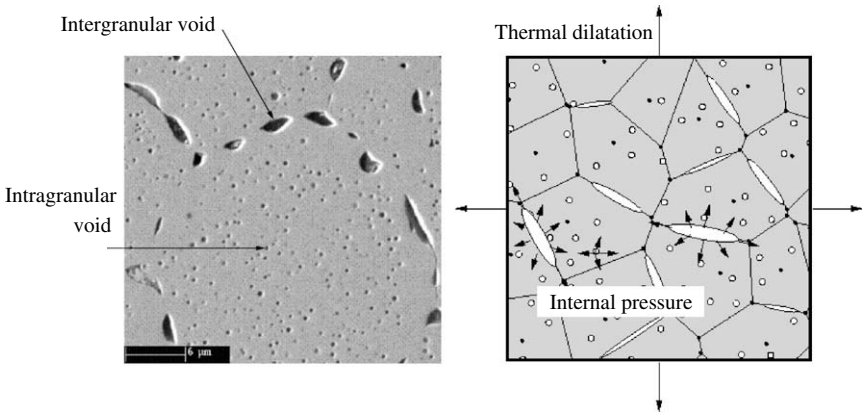

Fig. 1. (left) Micrography of irradiated UO_2 (33 GW j/T) after heat treatment at 2000 K during 3 h (Dubourg et al., 2005). (right) Swelling of UO_2 during an accident. Development of thermal strains and internal pressures inside the cavities.

scopic scale), a second population of cavities, roughly oblate spheroids with typical size of a few microns, can be observed at the grain boundaries (more information about the formation and growth of intragranular and intergranular fission gas bubbles in UO_2 can be found in Kashibe et al. (1993), Lösönen (2000), and Kashibe and Une, 1991). These voids are referred to as *intergranular voids*. Both types of cavities contain fission gases, with possibly different pressures in the intergranular and in the intragranular populations. Under postulated accident condition, the temperature in the material increases suddenly, resulting in a thermal dilatation of the material and in a sudden raise of the pressure of the gases contained in the cavities. At such high temperatures the polycrystalline ceramic is ductile and the two populations of cavities start growing until they eventually coalesce to form a macro-crack through which the fission gases find their way to the outer envelope (as schematically depicted in Fig. 1 right). The question addressed in the present study is the prediction of the critical overall thermal dilatation and critical internal pressures in the voids which can be sustained by the material before the formation of a macro-crack.

This problem bears a strong ressemblence with ductile rupture in metals and our study has several common points with earlier work in this domain. In particular, relations describing void growth by diffuse plasticity are obtained as an outcome of a constitutive model for elastoplastic materials containing two populations of voids, whereas coalescence is seen as the transition from a diffuse mode of plastic deformation into a localized mode. Therefore, the program of our study follows closely that of more classical studies in ductile fracture. In the first part of the study (this paper), the effective behavior of voided materials with two populations of pores of different size subjected to internal pressure is derived, the geometry and size of the pores *being fixed*. In the terminology of Ponte Castañeda and Zaidman (1996) and Zaidman and Ponte Castañeda (1996), we are interested here in *instantaneous constitutive relations*. In a second step (companion paper), we will be interested in the evolution of the microstructure described by differential equations for the geometrical parameters describing the shape and distribution of the voids in terms of the applied loading consisting of overall stresses and internal pressures.

There exists a huge body of literature devoted to the effective behavior of ductile voided materials originating from the seminal work of Gurson (1977) (see for instance Tvergaard, 1990; Pardoen and Hutchinson, 2000; Benzerga, 2002, and references therein for a review). However, several features of the present problem remain either untouched or only partially covered in the existing literature:

(1) *First, two populations of voids of different size co-exist in our material*. The presence of a second population of voids, has been experimentally observed by Marini et al. (1985) to influence the growth of larger voids in metals. From the standpoint of modelling, Perrin and Leblond (1990) gave an analytical solution for the response of a spherical void surrounded by a Gurson material under hydrostatic tension. Tvergaard (1998) assessed numerically the effect of a second population of void on the coalescence of a primary population, whereas Fabrègue and Pardoen (2008) extended the constitutive model of Pardoen and Hutchinson (2000) to voided materials with two populations of voids.

(2) *Second, both populations of voids are subjected to internal pressures* which can be different in the secondary and in the primary population. Consideration of internal pressure in plastically deforming voided materials is rather seldom in the literature with the noticeable exception of Dormieux et al. (2002). These authors make use of a micromechanical modelling which differs from the Gurson's line of thought and is based on the so-called *modified secant method* which is another name for the earlier *variational procedure* of Ponte Castañeda (1991).

(3) *Third, the larger voids are spheroidal, oblate and randomly oriented*, rather than spherical in shape. The Gurson's model, initially developed for spherical voids, has been extended to *aligned* spheroidal cavities, either prolate or oblate, by Gologanu et al. (1993) and Gologanu et al. (1994) who proposed improved velocity fields for ellipsoidal cavities generalizing the fields used by Gurson in his initial variational analysis. These improved velocity fields are used in the constitutive models of Pardoen and Hutchinson (2000) and Benzerga (2002) in the regime of void growth by general-

ized plasticity (generalized is to be understood here by contrast with localized plasticity). However, the matrix incompressibility plays a crucial role in these earlier analysis, since these velocity fields are divergence-free by construction. The presence of secondary voids requires the introduction of a compressible velocity field around the larger ellipsoidal voids and the present study shows how to combine these earlier incompressible fields with a dilatational field. Finally, the random orientation of the voids is also accounted for by means of averaging over orientation.

The present paper is organized as follows. Notations and more specific data about the material and its microstructure are given in Section 2. Then estimates for the poro-elastic properties of doubly voided materials are given in terms of the primary and secondary void volume-fractions in Section 3. The influence of the internal pressure in each population of voids is reflected in the overall stress through two Biot's tensors (one for each population of voids). The poro-plastic properties of doubly voided materials are investigated in Section 4 and 5. Upper bounds for the effective poro-plastic properties of doubly voided materials are derived in Section 4 using two classical approaches of the problem of voided materials, the Gurson-like approach and the variational procedure. The velocity fields proposed by Gologanu et al. (1994) are slightly modified to account for the matrix compressibility. To fill the gap between the two approaches, a *N*-phase model is proposed in Section 5. It is presented first in the case of two populations of spherical voids and extended to randomly oriented spheroidal voids. The accuracy of this *N*-phase model is assessed by comparison with FEM simulations.

Again, all microstructural information is assumed to be fixed in this first paper. The evolution of the microstructural parameters describing the arrangement of the voids (volume fraction, distribution and aspect ratio) will be discussed in the second part of the study.

2. Material and microstructural data

2.1. Matrix constitutive relations

The mechanical properties of non-irradiated UO_2 have been studied by Martin (1989) (linear elastic properties) and Canon et al. (1971) (non-linear range up to failure). Martin (1989) gives the Young modulus and the Poisson ratio of non-irradiated UO_2 as a function of the initial porosity and temperature. Regarding the full stress–strain curve of UO_2, experimental results reported in Canon et al. (1971) show that UO_2 exhibits a quasi-brittle behavior at low temperature (below 1000 °C), associated with a quasi-linear stress–strain curve up to failure. In this range of temperature, the maximal elongation (shown in Fig. 2, right) is small. The material ductility increases significantly above 1500 °C, where the maximal elongation reaches several percents (see again Fig. 2, right). The stress–strain curve above 1500 °C reported in Canon et al. (1971) (not shown here) is typical of ideal plasticity with a flat stress–strain curve after yielding which can be idealized as a plateau. Further experiments by Guerin (1975) (in compression) have shown that above 1100 °C the ultimate stress in non-irradiated UO_2 is only 5–10% larger than its initial yield stress, confirming the fact that in this range of temperature the material exhibits almost no hardening. In accident conditions, the temperature raises above 1500 °C and UO_2 can be considered as a ductile material with negligible hardening. It is idealized in this study as an ideally plastic von Mises material.

Although ceramics at high temperature exhibit rate-sensitivity effects in creep, viscoplasticity has been neglected in the present study for several reasons. It is indeed a common practice in the community of nuclear materials to consider that UO_2 has the same ultimate stress under accident conditions and under creep conditions at low strain-rate, meaning that rate-sensitivity effects are not significant. To give more substance to this approximation, we emphasize that the major problem addressed in the first part of the paper is the assessment of the maximal internal pressure in the voids which can be sustained by UO_2 before loosing its carrying capacity. It is therefore a limit load problem for which it is well known that the details of the material behavior prior to the ultimate stress do not matter. However, in the second part of the paper we develop a constitutive model and the question of rate-sensitivity arises again. As is well known, viscous deformation at high temperature

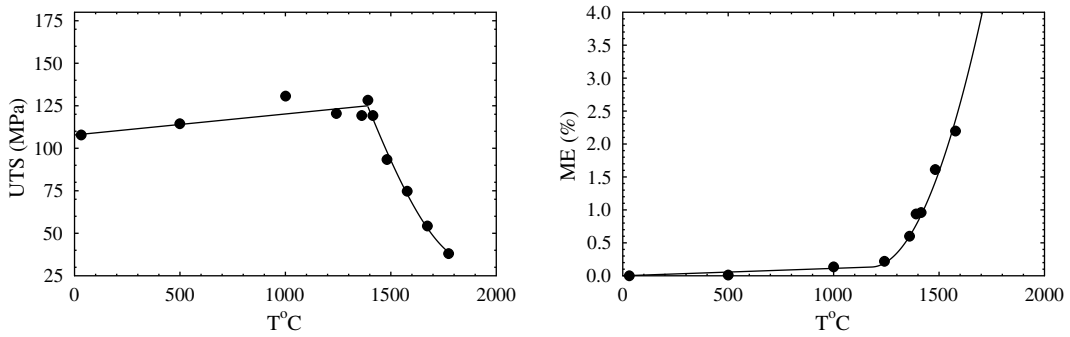

Fig. 2. Ultimate tensile stress (UTS) and maximal elongation (ME) versus temperature for non-irradiated UO_2 with 3% of initial porosity and 8 μm grain size (after Canon et al., 1971).

has two possible origins, vacancy diffusion and dislocation motion. Vacancy diffusion, which is the dominant mechanism in steady-state creep at high temperature corresponds to a rate-sensitivity exponent $n = 1$ (where the uniaxial viscous strain-rate $\dot{\varepsilon}^{vp}$ varies as σ^n). This mechanism is ruled out here by the very small time scale in accident conditions (about 30 μs). The only active mechanism is dislocation motion for which the rate-sensitivity exponent n is found in the literature to range between 4.5 and 17 (Guerin, 1975). A commonly accepted value is $n = 8$ (Monerie and Gatt, 2006) which, compared to $n = 1$ for diffusion, allows us to consider that viscosity effects are small. This observation has been summarized in Sauter and Leclercq (2003) by saying that "the behavior of uranium dioxide tends to be more plastic than viscous".

Let us finally add that most of the methods used in the present study can be extended to cover non-linear viscous behaviors of power-type just as Leblond et al. (1994) extended the analysis of Gurson to viscoplastic power-law materials. The local dissipation potentials as well as the final expressions of the effective potentials would be significantly different but the methods would be similar. Therefore, neglecting rate-sensitivity effects is admittedly an approximation, which, however, can be overcome using the methods put forward in this paper.

2.2. Scales and microstructure

The present problem with primary and secondary voids involves three different scales. The smallest (or microscopic) scale corresponds to the intragranular level (Fig. 1). The intermediate (or mesoscopic) scale corresponds to the scale of a single grain or of a couple of grains (Fig. 1). At this intermediate scale, the intragranular voids are small and their number is large. The intergranular voids are typically of mesoscopic size. The largest (or macroscopic) scale corresponds to a large representative volume element containing a sufficiently large number of grains and of intergranular voids and an even larger number of secondary voids. The difference in size of the two populations of voids (nanometers versus microns) is sufficient to consider the two scales as well-separated. Therefore, the up-scaling (or homogenization) procedure can be performed in two successive steps (see Fig. 3), first from the microscopic to the mesoscopic scale, smearing out all the small spherical voids, and second from the mesoscopic to the macroscopic scale, smearing out the details of the grain boundaries and the intergranular ellipsoidal voids. For conciseness the sound matrix at the microscopic scale will be denoted generically as M_0. This matrix contains spherical *intragranular* cavities with local porosity f_b. The first transition, from the microscopic to the mesoscopic scale, yields an effective medium corresponding to "M_0 + spherical voids" and denoted by M_1. The second transition from the mesoscopic scale to the macroscopic scale yields the effective properties of a heterogeneous material made of M_1 weakened by randomly oriented oblate (flat) spheroidal cavities with porosity f_e (*intergranular* cavities). The effective medium corresponding to "M_1 + oblate voids" is denoted by M_2. In most of this study, the intergranular cavities are assumed to be randomly located in space and randomly oriented. As can be seen in Fig. 1, their actual orientation is in fact not completely decorrelated from their spatial position, since they follow the grain boundaries. A more specific geometrical model, where each single grain is surrounded by a shell of softer material containing ellipsoidal voids, is investigated in the second part of this study.

Let V be a representative volume element at the larger scale; ω_e is the domain occupied by the intergranular cavities and ω_b is the domain occupied by the intragranular cavities. With these notations, the porosities f_b, f_e and the total porosity f can be expressed as

$$f_b = \frac{|\,\omega_b\,|}{|\,V-\omega_e\,|}, \quad f_e = \frac{|\,\omega_e\,|}{|\,V\,|}, \quad f = \frac{|\,\omega_e\,|+|\,\omega_b\,|}{|\,V\,|} = f_e + f_b(1-f_e). \tag{1}$$

2.3. Loading conditions

A sudden raise in pressure in the material results in three different components of the loading. First, the material is subjected to a thermal strain $\boldsymbol{E}$, which is usually an isotropic dilatation but which can be kept general. Then, the intragranular and intergranular voids are subjected to an internal pressure p_b and p_e, respectively, due to fission gases accumulated in

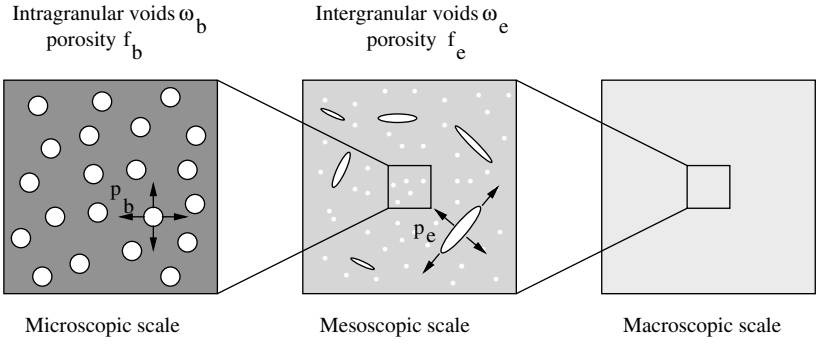

Fig. 3. Up-scaling (or homogenization) procedure.

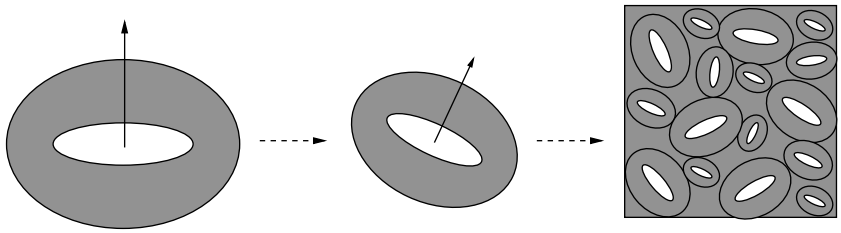

Fig. 4. Assemblage of self-similar randomly oriented hollow ellipsoids. Unit pattern (left). Rotated and dilated hollow ellipsoid (center). Representative volume element (right).

these cavities. p_b and p_e depend on several parameters (such as the volume of the voids) and can be different. To fix the terminology, when there is no internal pressure in the pores ($p_b = p_e = 0$) the material is said to be *drained*. In all the other cases (p_b or p_e different from 0), the material is said to be *saturated*.

2.4. Average stress and strain in voided materials

In the presence of voids, the definition of overall mechanical quantities usually defined as averages of microscopic ones, must be explicited. Since the homogenization procedure is performed in two steps, it is sufficient to consider here a single change of scales. Let V denote a representative volume element and ω denote the domain occupied by the voids (which could be ω_e or ω_b depending on the scale under consideration). The voids are subjected to a uniform internal pressure p. It is classical in all homogenization procedures to define the overall stress and strain as the volume averages of the corresponding local stress and strain fields over a representative volume element V:

$$\boldsymbol{\Sigma} = \langle \boldsymbol{\sigma} \rangle = \frac{1}{|V|}\left(\int_{V-\omega} \boldsymbol{\sigma}\, \mathrm{d}\boldsymbol{x} + \int_{\omega} \boldsymbol{\sigma}\, \mathrm{d}\boldsymbol{x} \right), \quad \boldsymbol{E} = \langle \boldsymbol{\varepsilon} \rangle = \frac{1}{|V|}\left(\int_{V-\omega} \boldsymbol{\varepsilon}\, \mathrm{d}\boldsymbol{x} + \int_{\omega} \boldsymbol{\varepsilon}\, \mathrm{d}\boldsymbol{x} \right). \tag{2}$$

However, the local stress and strain (or strain-rate) fields $\boldsymbol{\sigma}$ and $\boldsymbol{\varepsilon}$ are well defined only in the matrix $V - \omega$. The actual stress field, which is in equilibrium in the matrix and is in equilibrium with the pressure on the voids boundary can be continued inside ω by $-p\boldsymbol{i}$, where $\boldsymbol{i}$ stands for the second-order identity tensor. The corresponding overall stress reads as

$$\boldsymbol{\Sigma} = \langle \boldsymbol{\sigma} \rangle = -pf\boldsymbol{i} + \frac{1}{|V|}\int_{V-\omega} \boldsymbol{\sigma}\, \mathrm{d}\boldsymbol{x}, \tag{3}$$

where $f = |\,\omega\,| / |\,V\,|$. Similarly, the displacement field $\boldsymbol{u}$, which is well-defined in $V - \omega$, can be continued (in a non-unique manner) in a continuous displacement field inside ω. By doing so, the strain field in the matrix is continued in the voids by a compatible strain field. It remains to check that the average strain given by the second relation in Eq. (2) does not depend on the continuation chosen for $\boldsymbol{u}$. This is readily seen by integrating by part the integral over ω to get:

$$\boldsymbol{E} = \langle \boldsymbol{\varepsilon} \rangle = \frac{1}{|V|}\left(\int_{V-\omega} \boldsymbol{\varepsilon}\, \mathrm{d}\boldsymbol{x} - \int_{\partial\omega} \boldsymbol{u} \otimes_s \boldsymbol{n}\, \mathrm{d}s \right), \tag{4}$$

where $\boldsymbol{n}$ is the unit normal vector on the boundary of the voids pointing from the bulk material towards the interior of the void and where the symmetric tensorial product of $\boldsymbol{a}\otimes_s\boldsymbol{b}$ of the two vectors $\boldsymbol{a}$ and $\boldsymbol{b}$ is defined as $(a\otimes_s b)_{ij} = \frac{1}{2}(a_i b_j + a_j b_i)$. The relation Eq. (4) shows that the average strain $\boldsymbol{E}$ depends only on quantities (strain and displacement) defined in the matrix only, and does not depend on the choice of the continuation of $\boldsymbol{u}$ in ω.

3. Effective poro-elastic properties

This section is devoted to the effective elastic properties of voided materials subjected to internal pressure. Although the ultimate goal of this study is the modelling of a strongly non-linear problem, it is useful to begin with a linear problem for two reasons. First, because effective elastic moduli are required anyway for a complete modelling of the full process including both the elastic and the plastic response of the material. Second, because part of the non-linear theory which will be developed in the sequel makes use of a linear comparison composite and of its effective properties.

3.1. Biot tensor and Biot modulus for N-phase porous materials

This section presents more or less standard results about effective poro-elastic properties of N-phase voided materials (some of them can be found for two-phase materials in (Dormieux et al., 2002).

Consider a representative volume element V consisting of a matrix, itself subdivided into $N-1$ subphases with stiffness $\boldsymbol{C}^{(i)}$, occupying domains V_i, $i = 2, \ldots, N$ with volume fraction $f^{(i)}$ and saturated cavities occupying a domain $V_1 = \omega$ with volume fraction $f^{(1)} = f$ and subjected to internal pressure p. Only one population of voids is considered at this stage but the

procedure can be re-iterated if needed. Uniform strain conditions (among other possible boundary conditions, see Suquet, 1987 for a review) are applied on the boundary of V. The so-called *local problem* to be solved for the stress and displacement fields $\boldsymbol{\sigma}$ and $\boldsymbol{u}$ reads as

$$\begin{aligned} &\boldsymbol{\sigma} = \mathbf{C}^{(i)} : \boldsymbol{\varepsilon} \quad \text{in } V_i, \qquad \operatorname{div}(\boldsymbol{\sigma}) = \mathbf{0} \quad \text{in } V - \omega, \\ &\boldsymbol{\sigma} \cdot \boldsymbol{n} = -p \cdot \boldsymbol{n} \quad \text{on } \partial\omega, \qquad \boldsymbol{u} = \boldsymbol{E} \cdot \boldsymbol{x} \quad \text{on } \partial V. \end{aligned} \tag{5}$$

$\boldsymbol{n}$ the unit normal vector on the boundary of the voids pointing from the bulk material towards the interior of the void. Upon continuation of the local stress field $\boldsymbol{\sigma}$ by $-p\boldsymbol{i}$ inside ω, the extended field, still denoted by $\boldsymbol{\sigma}$, satisfies the equilibrium equations over the whole domain V. The constitutive equations of the phases

$$\boldsymbol{\sigma} = -p\boldsymbol{i} \text{ in phase 1}, \quad \boldsymbol{\sigma} = \mathbf{C}^{(i)} : \boldsymbol{\varepsilon} \text{ in phase } i, \ 2 \leqslant i \leqslant N,$$

can be rewritten as

$$\boldsymbol{\sigma} = \mathbf{C}^{(i)} : \boldsymbol{\varepsilon} + \boldsymbol{\tau}^{(i)}, \ 1 \leqslant i \leqslant N \quad \text{with } \mathbf{C}^{(1)} = \mathbf{0}, \ \boldsymbol{\tau}^{(1)} = -p\boldsymbol{i}, \ \boldsymbol{\tau}^{(i)} = \mathbf{0}, \ 2 \leqslant i \leqslant N. \tag{6}$$

With the above notations, a N-phase voided material subjected to internal pressure can be considered as a N-phase thermoelastic composite with energy

$$\boldsymbol{\sigma} = \frac{\partial w^{(i)}}{\partial \boldsymbol{\varepsilon}}(\boldsymbol{\varepsilon}), \quad w^{(i)}(\boldsymbol{\varepsilon}) = \frac{1}{2}\boldsymbol{\varepsilon} : \mathbf{C}^{(i)} : \boldsymbol{\varepsilon} + \boldsymbol{\tau}^{(i)} : \boldsymbol{\varepsilon}.$$

The general expression of the corresponding effective energy can be obtained by a general result about N-phase thermoelastic composites (Willis, 1981), that we recall here with standard notations

$$w^{\text{hom}}(\boldsymbol{E}) = \frac{1}{2}\boldsymbol{E} : \mathbf{C}^{\text{hom}} : \boldsymbol{E} + \boldsymbol{\tau}^{\text{hom}} : \boldsymbol{E} + \frac{1}{2} g^{\text{hom}}, \tag{7}$$

where

$$\mathbf{C}^{\text{hom}} = \sum_{i=1}^{N} f^{(i)} \mathbf{C}^{(i)} : \mathbf{A}^{(i)} = \mathbf{C}^{(N)} + \sum_{i=1}^{N-1} f^{(i)} (\mathbf{C}^{(i)} - \mathbf{C}^{(N)}) : \mathbf{A}^{(i)}, \tag{8}$$

$$\boldsymbol{\tau}^{\text{hom}} = \sum_{i=1}^{N} f^{(i)} \mathbf{A}^{(i)^T} : \boldsymbol{\tau}^{(i)}, \tag{9}$$

$$g^{\text{hom}} = \sum_{i=1}^{N} f^{(i)} \boldsymbol{\tau}^{(i)} : \boldsymbol{a}^{(i)}. \tag{10}$$

In the above relations, $\boldsymbol{I}$ is the fourth-order tensor representing the identity among symmetric second-order tensors, $f^{(i)}$ is the volume fraction of phase i, $\mathbf{A}^{(i)}$ is the (fourth-order) strain-localization tensor which relates the average strain in the ith phase to the macroscopic strain $\boldsymbol{E}$ in the absence of thermal stresses ($\boldsymbol{\tau}^{(i)} = \mathbf{0}, \ i = 1, \ldots N$) and $\boldsymbol{a}^{(i)}$ is the average strain in phase i due to the thermal stresses only ($\boldsymbol{E} = \mathbf{0}$).

Upon use of the expressions (6) in these relations, one obtains (with the change of notations $f^{(1)} = f$)

$$\boldsymbol{\tau}^{\text{hom}} = -pf\boldsymbol{i} : \mathbf{A}^{(1)}, \quad g^{\text{hom}} = -pf\boldsymbol{i} : \boldsymbol{a}^{(1)}. \tag{11}$$

Therefore, the effective energy of the N-phase composite can be put in the form

$$w^{\text{hom}}(\boldsymbol{E}, p) = \frac{1}{2}\boldsymbol{E} : \mathbf{C}^{\text{hom}} : \boldsymbol{E} - p\boldsymbol{B} : \boldsymbol{E} - \frac{1}{2}\frac{p^2}{M}, \tag{12}$$

where the second-order tensor $\boldsymbol{B}$ (Biot tensor) and the scalar M (Biot modulus) are given by

$$\boldsymbol{B} = f\boldsymbol{i} : \mathbf{A}^{(1)}, \quad \frac{1}{M} = \frac{f}{p}\boldsymbol{i} : \boldsymbol{a}^{(1)}. \tag{13}$$

The overall stress $\boldsymbol{\Sigma}$ being defined through (2) as the average stress (the stress field being extended by $-p\boldsymbol{i}$ in the voids), it can be shown by standard arguments to derive from the effective energy (12)

$$\boldsymbol{\Sigma} = \frac{\partial w^{\text{hom}}}{\partial \boldsymbol{E}}(\boldsymbol{E}, p) = \mathbf{C}^{\text{hom}} : \boldsymbol{E} - \boldsymbol{B}p. \tag{14}$$

3.2. Poro-elasticity of two-phase voided materials

The above expressions simplify further for two-phase composites ($N = 2$), phase 1 being the void phase, whereas the second phase is the homogeneous matrix. The localization operators can be explicitly expressed in terms of the effective stiffness $\mathbf{C}^{\text{hom}}$ of the composite

$$\boldsymbol{A}^{(1)} = \frac{1}{f^{(1)}}(\boldsymbol{C}^{(1)} - \boldsymbol{C}^{(2)})^{-1} : (\boldsymbol{C}^{\text{hom}} - \boldsymbol{C}^{(2)}),$$
$$\boldsymbol{a}^{(1)} = \frac{1}{f^{(1)}}(\boldsymbol{C}^{(1)} - \boldsymbol{C}^{(2)})^{-1} : (\boldsymbol{C}^{\text{hom}} - \langle \boldsymbol{C} \rangle) : (\boldsymbol{C}^{(1)} - \boldsymbol{C}^{(2)})^{-1} : (\boldsymbol{\tau}^{(1)} - \boldsymbol{\tau}^{(2)}),$$

and in the particular case of voided materials they reduce to

$$\boldsymbol{A}^{(1)} = \frac{1}{f}(\boldsymbol{I} - \boldsymbol{C}^{-1} : \boldsymbol{C}^{\text{hom}}), \quad \boldsymbol{a}^{(1)} = -\frac{p}{f}\boldsymbol{C}^{-1} : (\boldsymbol{C}^{\text{hom}} : \boldsymbol{C}^{-1} - (1-f)\boldsymbol{I}) : \boldsymbol{i},$$

where f is the void volume-fraction $f^{(1)}$ and $\boldsymbol{C}$ is the matrix stiffness. The corresponding expressions of the Biot tensor $\boldsymbol{B}$ and of the Biot modulus M for two-phase voided materials are

$$\boldsymbol{B} = (\boldsymbol{I} - \boldsymbol{C}^{\text{hom}} : \boldsymbol{C}^{-1}) : \boldsymbol{i} = \boldsymbol{i} : (\boldsymbol{I} - \boldsymbol{C}^{-1} : \boldsymbol{C}^{\text{hom}}), \quad \frac{1}{M} = \boldsymbol{i} : \boldsymbol{C}^{-1} : (\boldsymbol{B} - f\boldsymbol{i}). \tag{15}$$

These relations (which can also be found in Dormieux et al., 2006) show that *for two-phase materials* the Biot modulus is related to the Biot tensor. This is no longer the case in N-phase materials where we will have to resort to the general result (13).

When both the microstructure and the matrix are isotropic, the Biot tensor is an isotropic second-order tensor which reads as

$$\boldsymbol{B} = b\boldsymbol{i}, \quad b = 1 - \frac{k^{\text{hom}}}{k} \text{ and consequently } \frac{1}{M} = \frac{b-f}{k}, \tag{16}$$

where k and k^{hom} denote the bulk modulus of the matrix and of the effective medium, respectively.

3.3. First transition from the microscopic to the mesoscopic scale

The above general results can be applied successively to the two scale-transitions described in Section 2. Regarding the first transition, the specific material under consideration consists, at the microscopic scale, of an isotropic linear elastic matrix (with bulk and shear moduli denoted by k and μ, respectively) containing spherical voids (with porosity f_b) randomly distributed in the matrix. These voids are subjected to an internal pressure p_b. The relation (14) writes at the mesoscopic scale as

$$\boldsymbol{\Sigma} = \boldsymbol{C}_1^{\text{hom}} : \boldsymbol{E} - \boldsymbol{B}_1 p_b, \quad \boldsymbol{B}_1 = b_1\boldsymbol{i}, \ b_1 = 1 - \frac{k_1^{\text{hom}}}{k}, \tag{17}$$

where k and k_1^{hom} are the bulk moduli of the matrix M_0 at the microscopic scale and of the effective medium M_1 at the mesoscopic scale, respectively. It should be emphasized that the stress $\boldsymbol{\Sigma}$ in the relation (17) is the stress at the mesoscopic scale.

The effective stiffness $\boldsymbol{C}_1^{\text{hom}}$ of voided materials containing an isotropic distribution of spherical voids is known to be reasonably well-described by the Hashin–Shtrikman upper bound (Hashin and Shtrikman, 1963)

$$\frac{k_1^{\text{HS}}}{k} = \frac{(1-f_b)4\mu}{3kf_b + 4\mu}, \quad \frac{\mu_1^{\text{HS}}}{\mu} = \frac{(1-f_b)(9k+8\mu)}{(9+6f_b)k + 4(2+3f_b)\mu}, \quad b_1 = 1 - \frac{k_1^{\text{HS}}}{k}. \tag{18}$$

3.4. Second transition from the mesoscopic scale to the macroscopic scale

In the second scale transition, the domain V consists of a matrix whose constitutive relations are those of the mesoscopic effective medium M_1, weakened by randomly oriented oblate ellipsoidal cavities (domain ω_e, porosity f_e, aspect ratio w). V is subjected to uniform strain boundary conditions on its boundary ∂V and the voids are subjected to an internal pressure p_e. The local stress and strain fields solve the local problem

$$\begin{aligned} &\boldsymbol{\sigma} = \boldsymbol{C}_1^{\text{hom}} : \boldsymbol{\varepsilon} - b_1 p_b \boldsymbol{i} \quad \text{in } V - \omega_e, \qquad \text{div}(\boldsymbol{\sigma}) = \boldsymbol{0} \quad \text{in } V, \\ &\boldsymbol{\sigma} \cdot \boldsymbol{n} = -p_e \cdot \boldsymbol{n} \quad \text{on } \partial\omega_e, \qquad \boldsymbol{u} = \boldsymbol{E} \cdot \boldsymbol{x} \quad \text{on } \partial V. \end{aligned} \tag{19}$$

Note that, in these relations, the local stress field $\boldsymbol{\sigma}$ is the stress field at the mesoscopic scale and therefore corresponds to $\boldsymbol{\Sigma}$ in the relation (17). The change of variables

$$\boldsymbol{\sigma}^* = \boldsymbol{\sigma} + b_1 p_b \boldsymbol{i}$$

leads to

$$\begin{aligned} &\boldsymbol{\sigma}^* = \boldsymbol{C}_1^{\text{hom}} : \boldsymbol{\varepsilon} \quad \text{in } V - \omega_e, \qquad \text{div}(\boldsymbol{\sigma}^*) = \boldsymbol{0} \quad \text{in } V, \\ &\boldsymbol{\sigma}^* \cdot \boldsymbol{n} = (b_1 p_b - p_e) \cdot \boldsymbol{n} \quad \text{on } \partial\omega_e, \qquad \boldsymbol{u} = \boldsymbol{E} \cdot \boldsymbol{x} \quad \text{on } \partial V. \end{aligned} \tag{20}$$

A second use of the generic result (14) yields the following expression of $\boldsymbol{\Sigma}^* = \langle \boldsymbol{\sigma}^* \rangle_V$ (where the field $\boldsymbol{\sigma}^*$ has been extended by a uniform pressure field in ω_e):

$$\boldsymbol{\Sigma}^* = \boldsymbol{C}_2^{\text{hom}} : \boldsymbol{E} - \boldsymbol{B}_2(p_e - b_1 p_b). \tag{21}$$

The macroscopic stress $\boldsymbol{\Sigma}$, defined as $\langle \boldsymbol{\sigma} \rangle_V$ (where $\boldsymbol{\sigma}$ has been suitably extended by a uniform pressure field in ω_e) can consequently be expressed as

$$\boldsymbol{\Sigma} = \boldsymbol{C}_2^{\text{hom}} : \boldsymbol{E} - \boldsymbol{B}_2(p_e - b_1 p_b) - b_1 p_b \boldsymbol{i}. \tag{22}$$

The effective stiffness $\boldsymbol{C}_2^{\text{hom}}$ is estimated by a predictive scheme describing accurately the effective elastic properties of an isotropic matrix containing a random distribution of ellipsoidal voids. For this purpose, the upper bound of Ponte Castañeda and Willis (1995) will be adopted. The corresponding expressions of the bulk and shear moduli are given in Appendix A (where k and μ have to be replaced by k_1^{HS} and μ_1^{HS}). By virtue of the isotropy of the voided material at the macroscopic scale, the Biot tensor $\boldsymbol{B}_2$ is itself isotropic:

$$\boldsymbol{B}_2 = b_2 \boldsymbol{i}, \quad b_2 = 1 - \frac{k_2^{\text{PCW}}}{k_1^{\text{HS}}}, \tag{23}$$

where k_2^{PCW} is the bulk modulus given by the upper bound of Ponte Castañeda and Willis (1995). Finally, the relation (22) reduces to

$$\boldsymbol{\Sigma} = \boldsymbol{C}_2^{\text{PCW}} : \boldsymbol{E} - [b_2(p_e - b_1 p_b) + b_1 p_b]\boldsymbol{i}.$$

To conclude this section about the poro-elastic properties of porous materials with two populations of voids, we note that the present model requires the determination of two elastic moduli k_1^{HS} and μ_1^{HS} given by the relations (18), from which two other elastic moduli k_2^{PCW} and μ_2^{PCW} are given by the relations (A.3) and (A.6). The two Biot's coefficients b_1 and b_2 are given by the relations (18) and (23). Finally, in the elastic regime, the overall hydrostatic stress and the overall stress deviator can be expressed as

$$\Sigma_m = 3k_2^{\text{PCW}} E_m - b_2 p_e + (b_2 - 1) b_1 p_b, \quad \boldsymbol{\Sigma}^{\text{dev}} = 2\mu_2^{\text{PCW}} \boldsymbol{E}^{\text{dev}}, \tag{24}$$

where

$$\Sigma_m = \frac{1}{3}\Sigma_{ii}, \quad E_m = \frac{1}{3}E_{ii}, \quad \boldsymbol{\Sigma}^{\text{dev}} = \boldsymbol{\Sigma} - \Sigma_m \boldsymbol{i}, \quad \boldsymbol{E}^{\text{dev}} = \boldsymbol{E} - E_m \boldsymbol{i}.$$

For further use, it is also useful to introduce the equivalent stress and strain:

$$\Sigma_{\text{eq}} = \left(\frac{3}{2}\Sigma_{ij}^{\text{dev}}\Sigma_{ij}^{\text{dev}}\right)^{1/2}, \quad E_{\text{eq}} = \left(\frac{2}{3}E_{ij}^{\text{dev}}E_{ij}^{\text{dev}}\right)^{1/2}.$$

4. Poro-plasticity: upper bounds

4.1. Effective dissipation potential and effective flow surface

In the present section, the material is, at the microscopic scale, an incompressible, rigid ideally plastic matrix (von Mises criterion with yield stress σ_0). Elastic deformations are neglected and the question addressed here is the determination of the effective flow surface of porous materials containing two populations of voids. At this stage of the study, the microstructure is fixed, in other words, the two void volume-fractions f_b and f_e, the void aspect ratio w and the distribution of the voids are fixed.

Due to the difference in size of the two populations of voids, the homogenization process is performed into two successive steps. The smaller spherical voids are homogenized first and the resulting homogenized medium, denoted by M_1, corresponds to a compressible rigid-plastic material. This problem has been extensively studied in the literature and we shall rely on existing results for this first transition of scale (see Section 4.3) by adopting the Gurson–Tvergaard–Needleman model for M_1. Then a second transition of scales is performed, where the effective properties of a compressible rigid-plastic material M_1 containing randomly oriented ellipsoidal voids are estimated. Most of this section is devoted to this second scale transition. Our derivation is a combination of the two main lines of thought for the derivation of the effective properties of plastic porous materials from a micromechanical approach.

Both approaches are based on the minimization of the average plastic dissipation in a representative volume element under an imposed macroscopic strain-rate and the corresponding variational principle reads as

$$\boldsymbol{\Sigma} = \frac{\partial \Phi}{\partial \dot{\boldsymbol{E}}}(\dot{\boldsymbol{E}}, p), \quad \Phi(\dot{\boldsymbol{E}}, p) = \inf_{\dot{\boldsymbol{u}} \in \mathscr{K}(\dot{\boldsymbol{E}})} \frac{1}{|V|} \int_{V-\omega} \varphi(\boldsymbol{\varepsilon}(\dot{\boldsymbol{u}}))\mathrm{d}\boldsymbol{x} + p \int_{\partial\omega} \dot{\boldsymbol{u}} \cdot \boldsymbol{n}\,\mathrm{d}s, \tag{25}$$

where usually in the literature $p = 0$ (but not here). $\boldsymbol{\Sigma}$ and $\dot{\boldsymbol{E}}$ denote, respectively, the stress and strain-rate at the largest scale, $\mathcal{K}(\dot{\boldsymbol{E}})$ denotes the set of velocity fields $\dot{\boldsymbol{u}}$ satisfying $\dot{\boldsymbol{u}} = \dot{\boldsymbol{E}}.\boldsymbol{x}$ on ∂V, and φ is the dissipation potential of the matrix. The scale is not specified, as the variational principle (25) applies to both changes of scale (from the microscopic scale to the mesoscopic one, or from the mesoscopic scale to the macroscopic one). It should be noted that the dissipation potential φ, whose detailed expression depends on the problem at hand, is positively homogeneous of degree 1, i.e. satisfies

$$\varphi(\lambda\dot{\boldsymbol{\varepsilon}}) = \lambda\varphi(\dot{\boldsymbol{\varepsilon}}) \quad \text{for all positive } \lambda.$$

It can be readily checked that the overall potential Φ exhibits the same homogeneity of degree 1 as the local potential φ. As a result, an effective plasticity domain $P^{\text{hom}}(p)$ in which the macroscopic stress $\boldsymbol{\Sigma}$ is constrained to stay can be associated to the effective dissipation potential $\Phi(.,p)$. The domain $P^{\text{hom}}(p)$ is defined by

$$P^{\text{hom}}(p) = \{\boldsymbol{\Sigma} \text{ such that } \boldsymbol{\Sigma} : \dot{\boldsymbol{E}} \leqslant \Phi(\dot{\boldsymbol{E}}, p) \text{ for all } \dot{\boldsymbol{E}}\}. \tag{26}$$

The boundary of $P^{\text{hom}}(p)$ is the *effective flow surface* of the material and consists of all stresses deriving from the potential Φ:

$$\text{when } \dot{\boldsymbol{E}} \neq \boldsymbol{0}, \quad \boldsymbol{\Sigma} = \frac{\partial \Phi}{\partial \dot{\boldsymbol{E}}}(\dot{\boldsymbol{E}}, p) \text{ belongs to the effective flow surface.} \tag{27}$$

4.2. On bounding techniques for the effective potential

Two different approaches are classically followed in drained materials to obtain bounds or estimates for the effective potential of voided materials. The first approach finds its roots in the seminal paper of Gurson (1977) and consists in using the non-linear variational principle (25) with suitably chosen velocity fields. This procedure leads to an upper bound for the effective flow surface of the porous material under consideration, sharp bounds being obtained when the velocity fields used in the analysis are close approximations to the actual velocity fields in the volume element. The velocity fields originally used in Gurson's study of a single hollow sphere, were split into two contributions, one corresponding to a change of volume of the void without change in shape and the other part corresponding to a change in shape without change in volume. Gurson's velocity field has been generalized to more general geometries, but still sufficiently simple to be amenable to analytical calculations, to take advantage of, for instance, the incompressibility condition. To the best of the authors' knowledge the most general geometry for which accurate analytical velocity fields have been constructed is a hollow spheroidal domain delimited by two confocal spheroids (Gologanu et al., 1993; Gologanu et al., 1994).

The second line of thought follows the variational method of Ponte Castañeda (1991), which proceeds by transforming the non-linear variational problem into a variational problem for a *linear comparison composite (LCC)* with a corrective term accounting for the difference between the actual non-linear composite and the LCC. This variational method has been later interpreted by Suquet (1995) as a modified secant method where the effective strain in each individual phase is not the average strain over this phase but is related to its second moment (note that similar models based on second moments may also be found in Qiu and Weng (1992), Hu (1996) and Buryachenko (1996), with, however, no mention of the upper bound character of this modified secant method). The variational method can be easily extended to porous materials containing aligned, or randomly oriented, ellipsoidal voids and in fact to any microstructure for which an accurate predictive scheme is available for linear properties. This flexibility has allowed Ponte Castañeda and Zaidman (1996) to model microstructure evolution (change in void shape, orientation and distribution) in non-linearly viscous porous materials.

The two methods have different merits and different ranges of application. In the Gurson model, the first contribution to the velocity field is the exact velocity field in a hollow sphere under hydrostatic tension whereas the second contribution corresponds to a uniform strain-rate and is therefore far from reality. Not surprisingly, the Gurson model is accurate under hydrostatic stress, in the sense that its prediction coincides with the exact limit load of a hollow sphere (or any hollow sphere assemblage) under hydrostatic tension, $-\frac{2}{3}\sigma_0 \log f$ where f is the porosity, which can be considered as sharp. However, its prediction under purely deviatoric loading conditions, $\sigma_0(1-f)$, is the Voigt upper bound and is therefore likely to be a rather poor upper bound.

The situation for the variational method is opposite. The predictions, which have an upper bound character at all stress triaxialities, are accurate under purely deviatoric loading conditions (at least more accurate than that of the Gurson model) but are excessively high for hydrostatic loadings. In order to improve on these predictions for hydrostatic stress, Bilger et al. (2002) have proposed to consider the matrix as composed of N different phases, each phase corresponding to a thin spherical shell. In the LCC, each shell is assigned secant moduli which are different from those of the neighbouring shells. This procedure improves significantly on the predictions of the variational method (where the matrix is treated as a single phase). It recovers (when N is large enough) the exact result under hydrostatic loading (exact for a hollow sphere) and satisfies at all stress triaxialities the upper bound given by the variational method. The subdivision of the matrix into N subdomains, which accounts better for the strain heterogeneity in the matrix, will play an important role in our analysis.

4.3. First transition: von Mises matrix containing spherical voids

The problem considered in this first change of scale is that of a von Mises matrix containing a random distribution of spherical cavities subjected to an internal pressure p_b. In this first upscaling, the dissipation potential corresponds to the von Mises criterion

$$\varphi^{\mathrm{VM}}(\dot{\boldsymbol{\varepsilon}}) = \sigma_0 \dot{\varepsilon}_{\mathrm{eq}} \text{ when } \dot{\varepsilon}_m = 0, \quad \varphi^{\mathrm{VM}}(\dot{\boldsymbol{\varepsilon}}) = +\infty \text{ otherwise.}$$

4.3.1. Drained materials

In the case of *drained* materials where $p_b = 0$ (stress-free voids), the effective (mesoscopic) potential can be bounded from above by the potential

$$\varphi^{\mathrm{Gur}}(\dot{\boldsymbol{\varepsilon}}) = \sigma_0 \int_{q_1 f_b}^{1} \sqrt{\frac{4\dot{\varepsilon}_m^2}{y^2} + \frac{\dot{\varepsilon}_{\mathrm{eq}}^2}{q_3}}\, \mathrm{d}y, \tag{28}$$

and the corresponding flow surface is given (see Gărăjeu and Suquet, 1997 or Leblond, 2002) by the Gurson–Tvergaard–Needleman criterion (Gurson, 1977; Koplik and Needleman, 1988; Tvergaard, 1990)

$$q_3 \left(\frac{\Sigma_{\mathrm{eq}}}{\sigma_0}\right)^2 + 2q_1 f_b \cosh\left(\frac{3}{2}\frac{\Sigma_m}{\sigma_0}\right) - 1 - (q_1 f_b)^2 = 0, \tag{29}$$

where $\boldsymbol{\Sigma}$ is the mesoscopic stress. The coefficients q_1 and q_3, equal to 1 in the original analysis of Gurson, have been introduced by Needleman and Tvergaard to better reproduce unit-cell simulations. The parameter q_1 governs the critical porosity at which the material looses its carrying capacity and a range of recommended values for q_1 has been determined by Koplik and Needleman (1988) based on numerical simulations of the response of a cylindrical unit-cell containing an initially spherical void. The parameter q_3 determines the maximal shear which can be sustained by the voided material. A good agreement with finite element simulations and with existing bounds is obtained with

$$q_1 = 1.25, \quad q_3(f_b) = \left(1 + \frac{2}{3} f_b\right) \frac{(1 - q_1 f_b)^2}{(1 - f_b)^2}. \tag{30}$$

Leblond et al. (1994) have introduced the pre-factor $1 + \frac{2}{3} f_b$ in the expression of q_3 to satisfy the upper bound of Ponte Castañeda (1991) for a purely deviatoric loading $\left(\Sigma_{\mathrm{eq}} \leqslant \sigma_0 (1 - f_b)/\sqrt{1 + \frac{2}{3} f_b}\right)$. Although the values (30) are recommended, most of the present analysis remains valid with arbitrary q_1 and q_3.

4.3.2. Saturated materials

When the voids are *saturated* and subjected to an internal pressure p_b (identical in all voids), and *when the matrix is incompressible*, the mesoscopic flow surface of the medium M_1 is obtained from the flow surface of the drained case by a shift along the axis of hydrostatic stresses, Σ_m being replaced by $\Sigma_m + p_b$:

$$q_3 \left(\frac{\Sigma_{\mathrm{eq}}}{\sigma_0}\right)^2 + 2q_1 f_b \cosh\left(\frac{3}{2}\frac{\Sigma_m + p_b}{\sigma_0}\right) - 1 - (q_1 f_b)^2 = 0. \tag{31}$$

There are several possible proofs of (31). For instance, starting from the variational principle (25) with $\omega = \omega_b$ and $p = p_b$, one can note that the overall (mesoscopic) dilatation-rate reads as

$$3\dot{E}_m = \frac{1}{|V|} \int_{\partial V} \dot{\boldsymbol{u}} \cdot \boldsymbol{n}\, \mathrm{d}s = \frac{1}{|V|} \left(\int_{V - \omega_b} 3\dot{\varepsilon}_m\, \mathrm{d}\boldsymbol{x} - \int_{\partial \omega_b} \dot{\boldsymbol{u}} \cdot \boldsymbol{n}\, \mathrm{d}s \right).$$

It follows from this relation and from the matrix incompressibility that the last integral in (25) can be replaced by $-\mathrm{tr}\dot{\boldsymbol{E}}$. Finally, the overall (mesoscopic) stress in the drained case reads as

$$\boldsymbol{\Sigma} = \frac{\partial}{\partial \dot{\boldsymbol{E}}} \left(\inf_{\dot{\boldsymbol{u}} \in \mathscr{K}(\dot{\boldsymbol{E}})} \frac{1}{|V|} \int_{V - \omega_b} \varphi(\boldsymbol{\varepsilon}(\dot{\boldsymbol{u}}))\mathrm{d}\boldsymbol{x} - 3p_b \dot{E}_m \right) = \frac{\partial \Phi}{\partial \dot{\boldsymbol{E}}}(\dot{\boldsymbol{E}}, 0) - p_b \boldsymbol{i}, \tag{32}$$

where $\Phi(\dot{\boldsymbol{E}}, 0)$ is the effective potential in the drained case. In other words, when the matrix is incompressible at the microscopic scale, the stress $\boldsymbol{\Sigma}$ in the saturated material is such that $\boldsymbol{\Sigma} + p_b \boldsymbol{i}$ satisfies the effective constitutive equations for the *drained* material. In particular, in the case of a rigid-plastic matrix $\boldsymbol{\Sigma} + p_b \boldsymbol{i}$ satisfies the criterion (29). In addition, it follows from (32) that the mesoscopic effective potential satisfies

$$\Phi(\dot{\boldsymbol{E}}, p_b) = \Phi(\dot{\boldsymbol{E}}, 0) - 3p_b \dot{E}_m. \tag{33}$$

4.4. Second scale transition: randomly oriented spheroidal voids in a Gurson matrix

In the second transition of scales, the domain V consists of a matrix, which obeys the constitutive law M_1 derived by the first scale transition with a potential $\varphi(\dot{\boldsymbol{\varepsilon}}, p_b)$ and a random distribution of oblate ellipsoidal cavities with random orientation. The mesoscopic potential φ is obtained by the first scale transition and, according to the relation (33) satisfies

$$\varphi(\dot{\boldsymbol{\varepsilon}}, p_b) = \varphi(\dot{\boldsymbol{\varepsilon}}, 0) - 3p_b \dot{\varepsilon}_m = \varphi^{\mathrm{Gur}}(\dot{\boldsymbol{\varepsilon}}) - 3p_b \dot{\varepsilon}_m. \tag{34}$$

The domain occupied by the voids is ω_e with total porosity f_e, the void aspect-ratio (ratio between the vertical and the horizontal axis of the voids as shown in Fig. 17) is w and the internal pressure is p_e. The variational principle (25) then reads

$$\boldsymbol{\Sigma} = \frac{\partial \Phi}{\partial \dot{\boldsymbol{E}}}(\dot{\boldsymbol{E}}, p_b, p_e)$$

with

$$\Phi(\dot{\boldsymbol{E}}, p_b, p_e) = \inf_{\dot{\boldsymbol{u}} \in \mathscr{K}(\dot{\boldsymbol{E}})} \frac{1}{|V|}\left(\int_{V-\omega_e} \varphi(\boldsymbol{\varepsilon}(\dot{\boldsymbol{u}}), p_b)\mathrm{d}\boldsymbol{x} + p_e \int_{\partial\omega_e} \dot{\boldsymbol{u}} \cdot \boldsymbol{n}\,\mathrm{d}s\right).$$

The effective potential Φ can be expressed by means of (34) and of the relation

$$\frac{1}{|V|}\int_{V-\omega_e} 3\dot{\varepsilon}_m\,\mathrm{d}\boldsymbol{x} = 3\dot{E}_m + \frac{1}{|V|}\int_{\partial\omega_e} \dot{\boldsymbol{u}} \cdot \boldsymbol{n}\,\mathrm{d}s$$

as

$$\Phi(\dot{\boldsymbol{E}}, p_b, p_e) = \left[\inf_{\dot{\boldsymbol{u}} \in \mathscr{K}(\dot{\boldsymbol{E}})} \frac{1}{|V|}\left(\int_{V-\omega_e} \varphi^{\mathrm{Gur}}(\boldsymbol{\varepsilon}(\dot{\boldsymbol{u}}))\mathrm{d}\boldsymbol{x} + (p_e - p_b)\int_{\partial\omega_e} \dot{\boldsymbol{u}} \cdot \boldsymbol{n}\,\mathrm{d}s\right)\right] - 3p_b\dot{E}_m$$

or equivalently

$$\Phi(\dot{\boldsymbol{E}}, p_b, p_e) = \Phi(\dot{\boldsymbol{E}}, 0, p_e - p_b) - 3p_b\dot{E}_m. \tag{35}$$

In other words:

When the two populations of voids are saturated, with pressure p_b in the small voids and p_e in the large voids, and when the matrix is incompressible at the microscopic scale, it is sufficient to perform the second scale transition for a drained porous matrix ($p_b = 0$), provided that the pressure in the larger voids is set equal to $p^* = p_e - p_b$.

Regarding the local fields, the mesoscopic strain field in the actual saturated matrix is exactly that in the fictitious drained matrix whereas the stress field is shifted uniformly by $-p_b\boldsymbol{i}$ (as can be seen by inspecting the Euler–Lagrange equations associated with the variational principles defining $\Phi(\dot{\boldsymbol{E}}, p_b, p_e)$ and $\Phi(\dot{\boldsymbol{E}}, 0, p_e - p_b)$). The same shift applies to the overall macroscopic stress. Assuming that the second scale transition can be performed for a drained matrix and that the macroscopic stress $\boldsymbol{\Sigma}^*$ corresponding to an overall strain-rate $\dot{\boldsymbol{E}}$ is known, then the macroscopic stress in the actual saturated material is

$$\boldsymbol{\Sigma} = \boldsymbol{\Sigma}^* - p_b\boldsymbol{i}, \quad \boldsymbol{\Sigma}^* = \frac{\partial \Phi}{\partial \dot{\boldsymbol{E}}}(\dot{\boldsymbol{E}}, 0, p_e - p_b). \tag{36}$$

It is readily seen that the effective dissipation potential $\Phi(\dot{\boldsymbol{E}}, p_b, p_e)$ is a positively homogeneous function of degree 1 of the strain-rate $\dot{\boldsymbol{E}}$, independently of the internal pressures p_b or p_e. Thanks to the general result leading to (26) there exists an effective plasticity domain $P^{\mathrm{hom}}(p_b, p_e)$ depending on the two pressures p_b and p_e. The relation (36) implies that the plasticity domain $P^{\mathrm{hom}}(p_b, p_e)$ is obtained from the plasticity domain $P^{\mathrm{hom}}(0, p_e - p_b)$ corresponding to a drained matrix at the microscopic scale by a translation $-p_b\boldsymbol{i}$.

Another calculation, similar to that leading to (35), yields

$$\Phi(\dot{\boldsymbol{E}}, p_b, p_e) = \Phi(\dot{\boldsymbol{E}}, p_b - p_e, 0) - 3p_e\dot{E}_m.$$

Therefore, it is sufficient to determine the potential $\Phi(\dot{\boldsymbol{E}}, p_b - p_e, 0)$ corresponding to a saturated matrix (at the microscopic scale) weakened by drained ellipsoidal voids.

4.5. Second scale transition: an upper bound à la Gologanu

Thanks to the result (35), the small voids can be considered as stress-free in the rest of this section whereas the large voids are subjected to an internal pressure $p^* = p_e - p_b$, without loss of generality. It is sufficient to consider from now on the variational problem

$$\Phi(\dot{\boldsymbol{E}}, 0, p^*) = \inf_{\dot{\boldsymbol{u}} \in \mathscr{K}(\dot{\boldsymbol{E}})} \frac{1}{|V|}\left(\int_{V-\omega_e} \varphi^{\mathrm{Gur}}(\boldsymbol{\varepsilon}(\dot{\boldsymbol{u}}))\mathrm{d}\boldsymbol{x} + p^*\int_{\partial\omega_e} \dot{\boldsymbol{u}} \cdot \boldsymbol{n}\,\mathrm{d}s\right). \tag{37}$$

When $p^* = 0$ and when the matrix is a von Mises matrix, Gologanu et al. (1994) have proposed an incompressible velocity field for a special geometry of the elementary volume element in which the matrix occupies an ellipsoidal domain containing at its center an ellipsoidal void, the inner and outer surfaces being confocal ellipsoids. This velocity field, denoted by $\dot{\boldsymbol{u}}^{\mathrm{Gol}}$, satisfies the boundary condition $\dot{\boldsymbol{u}} = \dot{\boldsymbol{E}} \cdot \boldsymbol{x}$ on its outer boundary. Therefore, it can be extended to any volume V filled-in with an arbitrary assemblage of such self-similar hollow ellipsoids identical to the reference ellipsoid up to an arbitrary rotation and dilatation as shown in Fig. 4 (the filling-in process requires an infinite number of ellipsoids with smaller and smaller size). This velocity field is constructed sequentially as follows. First the field $\dot{\boldsymbol{u}}$ is set equal to $\dot{\boldsymbol{E}} \cdot \boldsymbol{x}$ in the whole domain V. Then a first ellipsoid is considered and the field is prescribed to be Gologanu et al. (1994)'s velocity field inside the ellipsoid

and $\dot{\boldsymbol{E}}\cdot\boldsymbol{x}$ outside. This field is continuous across the outer boundary of the ellipsoid. Then a second ellipsoid is considered and the same construction is repeated sequentially until the field is defined in all ellipsoids in the assemblage. The limit field (in the limit as all ellipsoids are taken into account) is continuous and satisfies $\dot{\boldsymbol{u}}=\dot{\boldsymbol{E}}\cdot\boldsymbol{x}$ on the outer boundary ∂V. However, the extended velocity fields inherit the incompressibility constraint present, by construction, in the field of Gologanu et al. (1994). Compressibility is introduced by adding to the incompressible velocity field $\dot{\boldsymbol{u}}^{\mathrm{Gol}}$ another contribution corresponding to a pure and uniform dilatation in the matrix

$$\dot{\boldsymbol{u}}=\dot{\boldsymbol{u}}^{\mathrm{Gol}}+A\boldsymbol{x},\quad \dot{\boldsymbol{\varepsilon}}=\dot{\boldsymbol{\varepsilon}}^{\mathrm{Gol}}+A\boldsymbol{i}.$$

The scalar A is a parameter which captures the average dilatation rate in the matrix (it is unlikely that the dilatation rate is uniform in the matrix, but it is expected that its average can be reasonably determined by using this type of trial field). The scalar A is determined through the variational property (37). The mean strain-rate and the equivalent strain-rate of the fields are related to those of Gologanu et al. (1994) by

$$\dot{\varepsilon}_m=A,\quad \dot{\varepsilon}_{\mathrm{eq}}=\dot{\varepsilon}_{\mathrm{eq}}^{\mathrm{Gol}},$$

and the corresponding expressions can be incorporated in (37) with (28). The computations, which follow in part the work of Gologanu et al. (1994) are a bit tedious and the reader is referred to Vincent et al. (2008) for more details. The result is that the effective potential can be bounded from above by

$$\Phi(\dot{\boldsymbol{E}},0,p^*)\leqslant\inf_{A}\left[\sigma_0\int_{q_1f_b}^{1}\int_{\lambda_1}^{\lambda_2}H(\lambda,A,y,\dot{E}_m,\dot{E}_{\mathrm{eq}})\mathrm{d}\lambda\,\mathrm{d}y-3p^*\dot{E}_m+3(1-f_e)p^*A\right],\tag{38}$$

where

$$H(\lambda,A,y,\dot{E}_m,\dot{E}_{\mathrm{eq}})=\sqrt{J^2(\lambda)\frac{4A^2}{y^2}+\frac{J(\lambda)}{q_3}(3Q_J(\lambda)(\dot{E}_m-A)^2+J(\lambda)\dot{E}_{\mathrm{eq}}^2)},\tag{39}$$

where the functions J, Q_J are given in Appendix B. λ is a geometric parameter attached to a continuous family of confocal ellipsoids varying between the outer and the inner boundaries of the hollow spheroid of reference defined, respectively, by $\lambda=\lambda_1$ and $\lambda=\lambda_2$ (see Fig. 17 in Appendix B). Again A represents the hydrostatic strain rate in the matrix and is determined by minimization of the plastic dissipation. Let us denote by A_{sol} the solution of this minimization problem. Using the relation (36), the effective flow surface for the saturated material with two pressure p_b and p_e is defined by the parametric equations

$$\begin{aligned}\Sigma_m&=-p_e+\frac{\sigma_0}{q_3}\int_{q_1f_b}^{1}\int_{\lambda_1}^{\lambda_2}\frac{J(\lambda)Q_J(\lambda)}{H(\lambda,A_{\mathrm{sol}},y,\dot{E}_m,\dot{E}_{\mathrm{eq}})}\mathrm{d}\lambda\,\mathrm{d}y(\dot{E}_m-A_{\mathrm{sol}}),\\ \Sigma_{\mathrm{eq}}&=\frac{\sigma_0}{q_3}\int_{q_1f_b}^{1}\int_{\lambda_1}^{\lambda_2}\frac{J^2(\lambda)}{H(\lambda,A_{\mathrm{sol}},y,\dot{E}_m,\dot{E}_{\mathrm{eq}})}\mathrm{d}\lambda\,\mathrm{d}y\,\dot{E}_{\mathrm{eq}}.\end{aligned}\tag{40}$$

As will be shown below, this upper bound is sharp for a purely hydrostatic loading but is rather inaccurate for purely deviatoric stresses. In the next section, an improved upper bound for purely deviatoric loadings is derived.

Remark. In the drained case ($p_b=p_e=0$), Vincent et al. (2008) have obtained an accurate analytical estimate of the yield criterion with $A=\frac{q_1f_b}{f_e+q_1f_b}\dot{E}_m$ (any choice of A delivers an upper bound).

4.6. Second scale transition: an upper bound based on the variational procedure of Ponte Castañeda

The second way to obtain bounds and estimates on the effective properties of porous media follows the variational approach of Ponte Castañeda (1991). Central to this technique is the notion of a LCC (see Ponte Castañeda and Suquet (1998)) which, here, exhibits the same geometry as the original non-linear material and whose properties are determined (optimally) by a non-linear closure condition. The LCC is composed of a linear matrix phase with stiffness $\boldsymbol{C}_0$ and its effective energy is added and substracted to the effective dissipation potential

$$\Phi(\dot{\boldsymbol{E}},0,p^*)\leqslant\inf_{\boldsymbol{C}_0\geqslant 0}(w_0^{\mathrm{hom}}(\dot{\boldsymbol{E}},p^*)+(1-f_e)\mathscr{V}_0(\boldsymbol{C}_0)),\tag{41}$$

where $w_0^{\mathrm{hom}}(\dot{\boldsymbol{E}},p^*)$ is the overall energy in the LCC whose expression is similar to (12) (with the strain replaced by the strain-rate)

$$\begin{aligned}w_0^{\mathrm{hom}}(\dot{\boldsymbol{E}},p^*)&=\inf_{\dot{\boldsymbol{u}}\in\mathscr{K}(\dot{\boldsymbol{E}})}\frac{1}{|V|}\left(\int_{V-\omega_e}\frac{1}{2}\boldsymbol{\varepsilon}(\dot{\boldsymbol{u}}):\boldsymbol{C}_0:\boldsymbol{\varepsilon}(\dot{\boldsymbol{u}})\mathrm{d}\boldsymbol{x}+p^*\int_{\partial\omega_e}\dot{\boldsymbol{u}}\cdot\boldsymbol{n}\,\mathrm{d}s\right)\\&=\frac{1}{2}\dot{\boldsymbol{E}}:\boldsymbol{C}_0^{\mathrm{hom}}:\dot{\boldsymbol{E}}-p^*\boldsymbol{B}:\dot{\boldsymbol{E}}-\frac{1}{2}\frac{(p^*)^2}{M}\end{aligned}\tag{42}$$

and $\mathscr{V}_0(\boldsymbol{C}_0)$ is defined as

$$\mathscr{V}_0(\boldsymbol{C}_0) = \sup_{\dot{\boldsymbol{\varepsilon}}} \left(\varphi^{\mathrm{Gur}}(\dot{\boldsymbol{\varepsilon}}) - \frac{1}{2}\dot{\boldsymbol{\varepsilon}} : \boldsymbol{C}_0 : \dot{\boldsymbol{\varepsilon}} \right).$$

Two properties of the effective properties of the LCC are worth noting. First, the Euler equations associated with the variational problem defining w_0^{hom} read as

$$\begin{aligned} &\boldsymbol{\sigma}^* = \boldsymbol{C}_0 : \dot{\boldsymbol{\varepsilon}} \quad \text{in } V - \omega_e, \qquad \mathrm{div}(\boldsymbol{\sigma}^*) = \boldsymbol{0} \quad \text{in } V, \\ &\boldsymbol{\sigma}^* \cdot \boldsymbol{n} = -p^* \boldsymbol{n} \quad \text{on } \partial\omega_e, \qquad \dot{\boldsymbol{u}} = \dot{\boldsymbol{E}} \cdot \boldsymbol{x} \quad \text{on } \partial V. \end{aligned} \tag{43}$$

Second, the second-moment of the strain-rate field on the matrix $M = V - \omega_e$ in the LCC can be computed from w_0^{hom} thanks to a general result for linear composites (Kreher and Pompe, 1985; Ponte Castañeda and Suquet, 1998)

$$\frac{1}{2}\langle \dot{\boldsymbol{\varepsilon}} \otimes \dot{\boldsymbol{\varepsilon}} \rangle_M = \frac{1}{|V - \omega_e|} \int_{V-\omega_e} \frac{1}{2} \dot{\boldsymbol{\varepsilon}} \otimes \dot{\boldsymbol{\varepsilon}} \, \mathrm{d}\boldsymbol{x} = \frac{1}{1 - f_e} \frac{\partial w_0^{\mathrm{hom}}}{\partial \boldsymbol{C}_0}(\dot{\boldsymbol{E}}, p^*). \tag{44}$$

Note that, in the expression of w_0^{hom} not only $\boldsymbol{C}_0^{\mathrm{hom}}$ but also the Biot coefficients $\boldsymbol{B}$ and M depend on $\boldsymbol{C}_0$ (this dependence is implicit). To obtain a more explicit form of $\mathscr{V}_0(\boldsymbol{C}_0)$ note that the Gurson potential, which is a function of $\dot{\varepsilon}_m^2$ and $\dot{\varepsilon}_{\mathrm{eq}}^2$ can be written in terms of the fourth-order tensor $\dot{\mathbf{e}}$:

$$\dot{\mathbf{e}} = \frac{1}{2}\dot{\boldsymbol{\varepsilon}} \otimes \dot{\boldsymbol{\varepsilon}}, \quad \dot{\varepsilon}_m^2 = \frac{2}{3}\boldsymbol{J} :: \dot{\mathbf{e}}, \quad \dot{\varepsilon}_{\mathrm{eq}}^2 = \frac{4}{3}\boldsymbol{K} :: \dot{\mathbf{e}} \quad \text{where } \boldsymbol{J} = \frac{1}{3}\boldsymbol{i} \otimes \boldsymbol{i}, \quad \boldsymbol{K} = \boldsymbol{I} - \boldsymbol{J},$$

and therefore

$$\varphi^{\mathrm{Gur}}(\dot{\boldsymbol{\varepsilon}}) = \phi^{\mathrm{Gur}}(\dot{\mathbf{e}}), \tag{45}$$

where ϕ^{Gur} is a convex function of $\dot{\mathbf{e}}$. Introducing the concave dual $(\phi^{\mathrm{Gur}})^*$ of ϕ^{Gur} one obtains that

$$\mathscr{V}_0(\boldsymbol{C}_0) = (\phi^{\mathrm{Gur}})^*(\boldsymbol{C}_0).$$

Then the optimality condition over $\boldsymbol{C}_0$ contained in (41) reads as

$$\frac{\partial w_0^{\mathrm{hom}}}{\partial \boldsymbol{C}_0}(\dot{\boldsymbol{E}}, p^*) = -(1 - f_e)\frac{\partial \mathscr{V}_0}{\partial \boldsymbol{C}_0}(\boldsymbol{C}_0) = -(1 - f_e)\frac{\partial (\phi^{\mathrm{Gur}})^*}{\partial \boldsymbol{C}_0}(\boldsymbol{C}_0).$$

In other words, the optimal moduli for the LCC are given by

$$\boldsymbol{C}_0 = \frac{\partial \phi^{\mathrm{Gur}}}{\partial \dot{\mathbf{e}}} \left(\frac{1}{1 - f_e} \frac{\partial w_0^{\mathrm{hom}}}{\partial \boldsymbol{C}_0}(\dot{\boldsymbol{E}}, p^*) \right) = \frac{\partial \phi^{\mathrm{Gur}}}{\partial \dot{\mathbf{e}}} \left(\frac{1}{2}\langle \dot{\boldsymbol{\varepsilon}} \otimes \dot{\boldsymbol{\varepsilon}} \rangle_M \right). \tag{46}$$

To *interpret* the operator $\partial\phi^{\mathrm{Gur}}/\partial\dot{\mathbf{e}}$, note that upon differentiation of the relation (45), one can write the stress–strain relation in the non-linear composite as

$$\boldsymbol{\sigma} = \frac{\partial \varphi^{\mathrm{Gur}}}{\partial \dot{\boldsymbol{\varepsilon}}}(\dot{\boldsymbol{\varepsilon}}) = \frac{\partial \phi^{\mathrm{Gur}}}{\partial \dot{\mathbf{e}}}(\dot{\mathbf{e}}) : \dot{\boldsymbol{\varepsilon}}.$$

Therefore, $\partial\phi^{\mathrm{Gur}}/\partial\dot{\mathbf{e}}$ is the fourth-order tensor of the *secant moduli* for a Gurson material. The final interpretation of the optimal elastic moduli in the LCC is that they are given by the secant moduli in a Gurson material, computed at the second moments of the strain-rate field in the LCC, which depend themselves on the elastic moduli of the LCC through (44). The consistency between (46) and (44) defines precisely the closure conditions for the the elastic moduli. In practice, the resulting non-linear problem is solved using a fixed-point algorithm

$$\left.\begin{array}{lcl} & & \dot{\boldsymbol{E}} \text{ being prescribed :} \\ \textit{Initialization} & : & \langle \dot{\mathbf{e}} \rangle_M^0 = \frac{1}{2}\dot{\boldsymbol{E}} \otimes \dot{\boldsymbol{E}}. \\ \textit{Iterate } k & : & \textit{Do until convergence :} \\ & & \boldsymbol{C}_0^k = \dfrac{\partial \varphi^{\mathrm{Gur}}}{\partial \dot{\mathbf{e}}}(\langle \dot{\mathbf{e}} \rangle_M^{k-1}), \quad \langle \dot{\mathbf{e}} \rangle_M^k = \dfrac{1}{1 - f_e}\dfrac{\partial w_0^{\mathrm{hom}}}{\partial \boldsymbol{C}_0^k}(\dot{\boldsymbol{E}}, p^*) \\ & & \textit{Enddo} \\ \textit{Output} & : & \boldsymbol{\Sigma}^* = \boldsymbol{C}_0^{\mathrm{hom}} : \dot{\boldsymbol{E}} - \boldsymbol{B}p^*. \end{array}\right\} \tag{47}$$

Convergence is reached when the difference between two iterates is small $\|\langle \dot{\mathbf{e}} \rangle_M^k - \langle \dot{\mathbf{e}} \rangle_M^{k-1}\| \leqslant \delta \|\langle \dot{\mathbf{e}} \rangle_M^k\|$ with $\delta = 10^{-2}$.

Once the secant modulus $\boldsymbol{C}_0$ of the matrix in the LCC is determined (after convergence of the above algorithm), the effective stiffness $\boldsymbol{C}_0^{\mathrm{hom}}$ of the LCC is estimated by means of the linear upper bound of Ponte Castañeda and Willis (1995). The resulting prediction is a rigorous upper bound for the effective non-linear behavior of the material Ponte Castañeda and Suquet (1998).

Owing to the matrix isotropy and to the random orientation of the ellipsoidal voids, the LCC is isotropic and this has two consequences. First its Biot tensor $\boldsymbol{B}$ and its Biot modulus $1/M$ read as

$$\boldsymbol{B} = b\boldsymbol{i} = \left(1 - \frac{k_0^{\mathrm{PCW}}}{k_0}\right)\boldsymbol{i}, \quad \frac{1}{M} = \frac{b - f_e}{k_0}.$$

Second, the only second-moments which matter for the determination of the LCC are the two invariants

$$\frac{2}{3}\langle\dot{\boldsymbol{e}}\rangle_M :: \boldsymbol{J} = \langle\dot{\varepsilon}_m^2\rangle_M, \quad \frac{4}{3}\langle\dot{\boldsymbol{e}}\rangle_M :: \boldsymbol{K} = \langle\dot{\varepsilon}_{\mathrm{eq}}^2\rangle_M.$$

The relation (44) reduces to

$$\begin{aligned}
\langle\dot{\varepsilon}_m^2\rangle_M &= \frac{1}{1-f_e}\frac{\partial k_0^{\mathrm{hom}}}{\partial k_0}\dot{E}_m^2 + \frac{1}{3(1-f_e)}\frac{\partial \mu_0^{\mathrm{hom}}}{\partial k_0}\dot{E}_{\mathrm{eq}}^2 - \frac{2p^*}{3(1-f_e)}\dot{E}_m\frac{\partial b}{\partial k_0} - \frac{(p^*)^2}{9(1-f_e)}\frac{\partial M^{-1}}{\partial k_0}, \\
\langle\dot{\varepsilon}_{\mathrm{eq}}^2\rangle_M &= \frac{3}{1-f_e}\frac{\partial k_0^{\mathrm{hom}}}{\partial \mu_0}\dot{E}_m^2 + \frac{1}{1-f_e}\frac{\partial \mu_0^{\mathrm{hom}}}{\partial \mu_0}\dot{E}_{\mathrm{eq}}^2 - \frac{2p^*}{1-f_e}\dot{E}_m\frac{\partial b}{\partial \mu_0} - \frac{(p^*)^2}{3(1-f_e)}\frac{\partial M^{-1}}{\partial \mu_0}.
\end{aligned} \tag{48}$$

Similarly, owing to the matrix isotropy, the fourth-order tensor $\boldsymbol{C}_0$ of secant moduli is characterized by a bulk and a shear modulus

$$\begin{aligned}
k_0 &= \frac{2}{9}\frac{\sigma_0}{\sqrt{\langle\dot{\varepsilon}_m^2\rangle_M}}\left(-\mathrm{Arcsinh}\left(2\sqrt{\frac{\langle\dot{\varepsilon}_m^2\rangle_M}{\langle\dot{\varepsilon}_{\mathrm{eq}}^2\rangle_M}q_3}\right) + \mathrm{Arcsinh}\left(\frac{2}{q_1 f_b}\sqrt{\frac{\langle\dot{\varepsilon}_m^2\rangle_M}{\langle\dot{\varepsilon}_{\mathrm{eq}}^2\rangle_M}q_3}\right)\right), \\
\mu_0 &= \frac{1}{3}\frac{\sigma_0}{\langle\dot{\varepsilon}_{\mathrm{eq}}^2\rangle_M}\left(\sqrt{4\langle\dot{\varepsilon}_m^2\rangle_M + \frac{\langle\dot{\varepsilon}_{\mathrm{eq}}^2\rangle_M}{q_3}} - q_1 f_b\sqrt{\frac{4\langle\dot{\varepsilon}_m^2\rangle_M}{(q_1 f_b)^2} + \frac{\langle\dot{\varepsilon}_{\mathrm{eq}}^2\rangle_M}{q_3}}\right).
\end{aligned} \tag{49}$$

The fixed-point algorithm (47) takes a simpler form where the unknown fourth-order tensor $\langle\dot{\boldsymbol{e}}\rangle_M$ is replaced by the two scalars $\langle\dot{\varepsilon}_m^2\rangle_M$ and $\langle\dot{\varepsilon}_{\mathrm{eq}}^2\rangle_M$ and the two tensorial relations in (47) are replaced by the two sets of scalar Eqs. (49) and (48).

Finally, the overall stress $\boldsymbol{\Sigma}^*$ in the drained material is given by (47) and the actual stress in the saturated material $\boldsymbol{\Sigma} = \boldsymbol{\Sigma}^* - p_b\boldsymbol{i}$ reads as

$$\boldsymbol{\Sigma} = \Sigma_m\boldsymbol{i} + \frac{2}{3}\Sigma_{\mathrm{eq}}\frac{\dot{\boldsymbol{E}}^{\mathrm{dev}}}{\dot{E}_{\mathrm{eq}}}, \quad \Sigma_m = 3k_0^{\mathrm{PCW}}\dot{E}_m + (p_e - p_b)\frac{k_0^{\mathrm{PCW}}}{k_0} - p_e, \quad \Sigma_{\mathrm{eq}} = 3\mu_0^{\mathrm{PCW}}\dot{E}_{\mathrm{eq}}. \tag{50}$$

The moduli k_0^{PCW} and μ_0^{PCW} are given in Appendix A. The derivatives of these moduli with respect to the elastic moduli of the matrix can be obtained explicitly using a symbolic computation software but are too complicated to be given in this document.

We emphasize the fact that, once convergence is reached, the expression (42) is a rigorous upper bound for the potential (37).

4.7. Comparison between the two upper bounds. Orientation of the next section

The two upper bounds (40) and (50) are compared in Fig. 5 for a drained porous material ($p_b = p_e = 0$) containing two populations of spherical voids ($f_e = 0.1$, $f_b = 0.01$). They are also compared with the exact result of Perrin (1992) (which is recalled in Appendix D and extended to saturated pores). As already observed by different authors (in particular Leblond et al., 1994; Bilger et al., 2002) the bound given by the variational method is too large for hydrostatic loadings whereas the bound given by a suitably chosen velocity field (in the spirit of Gurson's analysis) is sharp in this case. The situation is opposite for purely deviatoric loadings where the upper bound derived from the variational method is more accurate than the

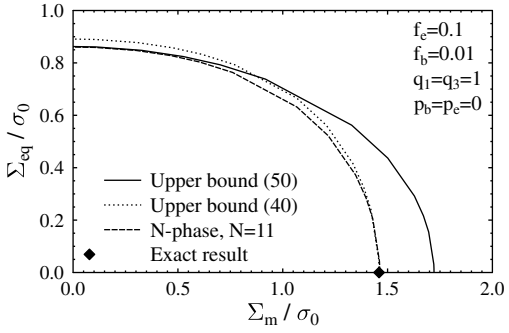

Fig. 5. Spherical voids in a Gurson matrix. $f_e = 0.1$, $f_b = 0.01$, $q_3 = q_1 = 1$. Drained case ($p_b = p_e = 0$). Comparison between different predictions: upper bound (40) (dotted line), upper bound (50) (solid line), N-phase model ($N = 11$, dashed line), exact result (D.7) for hydrostatic loading (diamond).

bound given by the Gurson-like approach. This is not surprising since the Gurson-like bound coincides with the crude Voigt bound for purely deviatoric loadings. To improve on both bounds, a N-phase model is presented in the next section in the spirit of the N-phase model of Bilger et al. (2002).

5. Poro-plasticity: a N-phase model

5.1. Voided materials with two populations of spherical voids

5.1.1. Coated spheres

When both the intragranular and intergranular voids are spherical in shape, an improvement on the prediction of the preceding section can be brought by considering the LCC as a N-phase composite, rather than as a two-phase medium. This is in line with the work of Bilger et al. (2002). Consider a hollow sphere (or an assemblage of hollow spheres) where the matrix is subdivided into $N-1$ concentric spherical shells Ω_i, $2 \leqslant i \leqslant N$ surrounding the central cavity (phase 1). Each subdomain Ω_i with volume fraction f_i is occupied by an elastic material with different moduli $k_0^{(i)}$ and $\mu_0^{(i)}$ (see Fig. 6 left).

The non-linear problem which is to be solved to determine the optimal LCC consists in solving a set of $4N$ non-linear equations in each phase using a fixed-point algorithm similar to (47). The four equations in each phase are very similar to Eqs. (48) and (49). In the interest of space these equations are not explicitly given here but they consist in replacing the elastic moduli of the matrix k_0 and μ_0 by $k_0^{(i)}$ and $\mu_0^{(i)}$ in each layer ($i = 2, \ldots, N$) and the second moments $\langle \dot{\varepsilon}_m^2 \rangle_M$ and $\langle \dot{\varepsilon}_{\mathrm{eq}}^2 \rangle_M$ by $\langle \dot{\varepsilon}_m^2 \rangle_i$ and $\langle \dot{\varepsilon}_{\mathrm{eq}}^2 \rangle_i$ where $\langle \cdot \rangle_i$ denotes the volume averaging over Ω_i. The secant moduli $k_0^{(i)}$ and $\mu_0^{(i)}$ are deduced from the second moments $\langle \dot{\varepsilon}_m^2 \rangle_i$ and $\langle \dot{\varepsilon}_{\mathrm{eq}}^2 \rangle_i$ by the relation (49), whereas the second moments in phase i of the strain-rate field $\langle \dot{\varepsilon}_m^2 \rangle_i$ and $\langle \dot{\varepsilon}_{\mathrm{eq}}^2 \rangle_i$ are obtained by derivation of the overall effective energy with respect to the elastic moduli of phase i. The non-linear equations to be solved read as

$$
\begin{aligned}
k_0^{(i)} &= \frac{2}{9}\sigma_0 \frac{1}{\sqrt{\langle \dot{\varepsilon}_m^2 \rangle_i}} \left(-\mathrm{Arcsinh}\left(2\sqrt{\frac{\langle \dot{\varepsilon}_m^2 \rangle_i}{\langle \dot{\varepsilon}_{\mathrm{eq}}^2 \rangle_i}} q_3 \right) + \mathrm{Arcsinh}\left(\frac{2}{q_1 f_b} \sqrt{\frac{\langle \dot{\varepsilon}_m^2 \rangle_i}{\langle \dot{\varepsilon}_{\mathrm{eq}}^2 \rangle_i}} q_3 \right) \right), \\
\mu_0^{(i)} &= \frac{1}{3}\frac{\sigma_0}{\langle \dot{\varepsilon}_{\mathrm{eq}}^2 \rangle_i} \left(\sqrt{4\langle \dot{\varepsilon}_m^2 \rangle_i + \frac{\langle \dot{\varepsilon}_{\mathrm{eq}}^2 \rangle_i}{q_3}} - q_1 f_b \sqrt{\frac{4\langle \dot{\varepsilon}_m^2 \rangle_i}{(q_1 f_b)^2} + \frac{\langle \dot{\varepsilon}_{\mathrm{eq}}^2 \rangle_i}{q_3}} \right), \\
\langle \dot{\varepsilon}_m^2 \rangle_i &= \frac{1}{f_i}\frac{\partial k_0^{\mathrm{hom}}}{\partial k_0^{(i)}} \dot{E}_m^2 + \frac{1}{3f_i}\frac{\partial \mu_0^{\mathrm{hom}}}{\partial k_0^{(i)}} \dot{E}_{\mathrm{eq}}^2 - \frac{2p^*}{3f_i}\dot{E}_m \frac{\partial b}{\partial k_0^{(i)}} - \frac{(p^*)^2}{9f_i}\frac{\partial M^{-1}}{\partial k_0^{(i)}}, \\
\langle \dot{\varepsilon}_{\mathrm{eq}}^2 \rangle_i &= \frac{3}{f_i}\frac{\partial k_0^{\mathrm{hom}}}{\partial \mu_0^{(i)}} \dot{E}_m^2 + \frac{1}{f_i}\frac{\partial \mu_0^{\mathrm{hom}}}{\partial \mu_0^{(i)}} \dot{E}_{\mathrm{eq}}^2 - \frac{2p^*}{f_i}\dot{E}_m \frac{\partial b}{\partial \mu_0^{(i)}} - \frac{(p^*)^2}{3f_i}\frac{\partial M^{-1}}{\partial \mu_0^{(i)}}.
\end{aligned}
\tag{51}
$$

The overall poro-elastic moduli k_0^{hom}, μ_0^{hom}, b and M can be estimated by the N-phase self-consistent scheme of Hervé and Zaoui (1993) recalled and extended to poro-elastic constituents in Appendix C. The effective moduli are denoted by k_0^{HZ} and μ_0^{HZ}, b and M. With these, the coupled non-linear Eq. (51) are solved using a fixed-point algorithm which is a straightforward generalization of Eq. (47) to a N-phase composite.

5.1.2. Influence of the number N of subdomains

The predictions of the model depend on the number N of phases. The results for $N = 2$ (almost) coincide with the variational upper bound of Section 4.6 (the only difference being that here the self-consistent scheme is used instead of the PCW upper bound) and are therefore inaccurate under hydrostatic loadings (see Fig. 6). At the other end, $N = \infty$ reproduces exactly the analytical limit load of a single hollow sphere under hydrostatic loading.

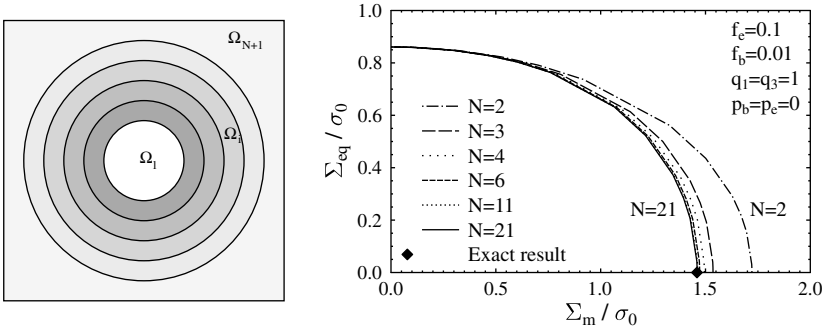

Fig. 6. (left) Multi-layered inclusion in an infinite matrix. (right) Influence of the number of subdomains on the accuracy of the N-phase model. $f_e = 0.1$, $f_b = 0.01$, $q_3 = q_1 = 1$. Drained case ($p_b = p_e = 0$). Diamond: exact result (D.7).

To assess the effect of the number N of layers, all layers are assigned the same thickness and N is varied. As can be seen in Fig. 6, the predictions for $N = 6,\ 11,\ 21$ fall almost on top of each other and are in very good agreement with the analytical solution (Perrin, 1992) for a Gurson matrix containing a stress-free central void and subjected to hydrostatic tension. In view of these results, it can be considered that $N = 6$ achieves a good compromise between accuracy and computational cost when the computational cost is a concern. In other cases, any N larger than 6 yields accurate results. Similarly, when the voids are saturated, the predictions of the N-phase model can be compared to the two analytical results (D.7) for hydrostatic loading. The agreement is again excellent as can be seen in Fig. 7 even when the number of layers is moderate ($N = 6$ in the results shown).

5.1.3. Comparison with the upper bounds and with finite element simulations

Fig. 5 shows that the predictions of the N-phase model respect the two upper bounds (40) and (50) coinciding with the best bound at zero or infinite stress-triaxiality ratio. Therefore the N-phase model is a good compromise at arbitrary stress-triaxiality ratio.

The predictions of the N-phase estimate for the effective yield surface of a bi-porous material are compared in Fig. 9 with full-field numerical simulations performed with the finite element method. Attention is limited here to axisymmetric deformations, one quarter of a hollow sphere is meshed and boundary conditions corresponding to uniform deformations are imposed on the outer boundary of the hollow sphere. The matrix is a Gurson material (with $q_1 = q_3 = 1$) and simulations have been carried out with two different values of the porosity $f_b = 0.01$ and $f_b = 0.1$. Two different values of the porosity f_e have been considered: $f_e = 0.01$ and $f_e = 0.1$. The meshes used in the simulations are shown in Fig. 8 (quadratic elements).

Different radial paths in the space of macroscopic stress are followed using a stress-driven method similar to that described in Michel et al. (1999). Briefly, the outer boundary of the hollow sphere is subjected to an imposed displacement corresponding to a uniform strain-rate $\dot{\boldsymbol{u}} = \dot{\boldsymbol{E}}.\boldsymbol{x}$ on $\partial\Omega$ where the overall strain-rate $\dot{\boldsymbol{E}}$ is unknown and is determined iteratively by requesting the overall stress to be aligned with the imposed stress direction.

Fig. 9 shows a good agreement between the estimate (with $N = 21$) and the numerical simulations. The shapes of the yield surfaces are similar and the predictions under purely hydrostatic and purely deviatoric stress are almost on top of each other.

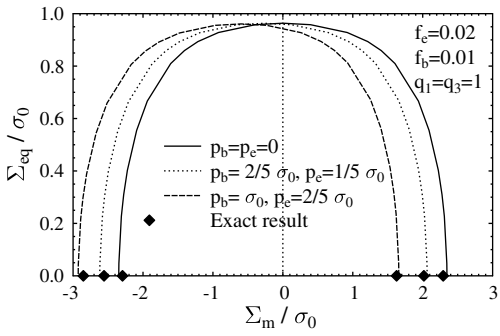

Fig. 7. Effective flow surface of porous materials containing two populations of spherical voids. Influence of the internal pressures on the effective yield surface. N-phase estimate ($N = 6$), $f_e = 0.02$, $f_b = 0.01$, $q_3 = q_1 = 1$. Diamond: exact result (D.7). Drained case ($p_b = p_e = 0$) and saturated cases: $p_b = (2/5)\sigma_0$, $p_e = (1/5)\sigma_0$, and $p_b = \sigma_0$, $p_e = (2/5)\sigma_0$.

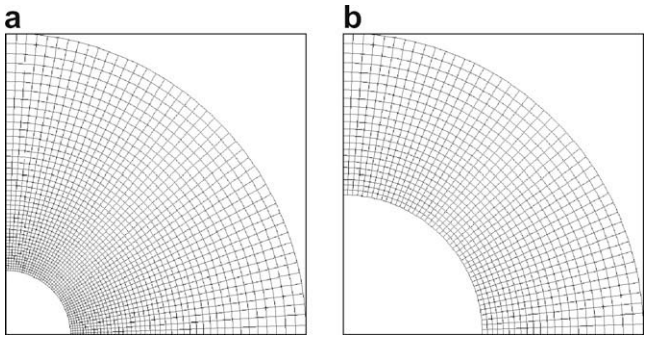

Fig. 8. Finite element meshes used in the unit-cell calculations: (a) $f_e = 0.01$, (b) $f_e = 0.1$.

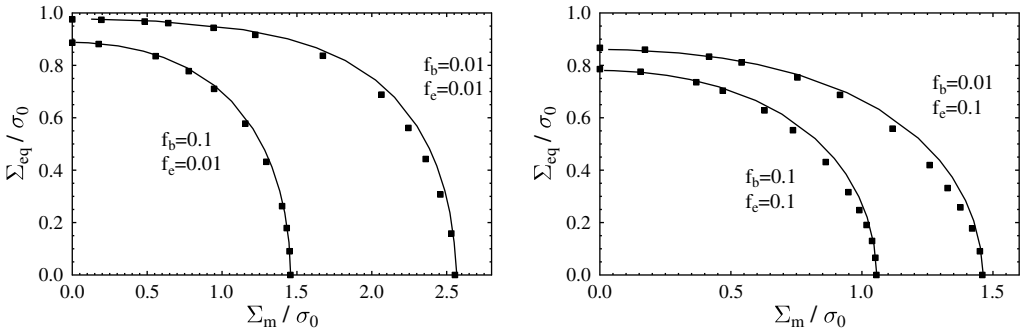

Fig. 9. Spherical voids in a Gurson matrix. Finite elements simulations (black squares) and N-phase estimate ($N = 21$, solid line), $q_3 = q_1 = 1$. Drained case ($p_b = p_e = 0$).

5.2. Gurson matrix weakened by randomly oriented ellipsoidal voids

5.2.1. A N-phase model

When the intergranular voids are oblate ellipsoids characterized by their volume fraction f_e and their aspect ratio w (see Appendix B), and when the microstructure is an assemblage of such self-similar ellipsoids with random orientation, the most natural generalization of the N-phase model would be to consider a subdivision of the matrix in a single hollow ellipsoid into $N-1$ ellipsoidal shells, as schematized in Fig. 10 left. Unfortunately, the exact solution to the elasticity problem for the N-phase LCC with embedded ellipsoids is not known to the best of the authors' knowledge and we must resort to an approximate resolution. The approximation that will be retained in the rest of this study is based on the following idea of "equivalent spherical porosities". Suppose that the LCC with ellipsoidal voids (porosity f_e, aspect ratio w, Fig. 10 left) can be replaced by an "equivalent" LCC with spherical voids (porosity f_s, Fig. 10 right). The N-phase model can be applied to the equivalent LCC instead of the real one. The two composites (the one with ellipsoidal voids and the one with spherical voids) will be considered as equivalent if all the poro-elastic effective moduli coincide in the two composites.

To define more precisely this equivalence, let us go back to the case $N = 2$ where the matrix is considered as a single phase. In the case of the actual composite with ellipsoidal voids the effective moduli denoted by $k^{\hom}_{\text{ellips}}(f_e, w)$, $\mu^{\hom}_{\text{ellips}}(f_e, w)$, $b_{\text{ellips}}(f_e, w)$ and $M_{\text{ellips}}(f_e, w)$ for clarity, are estimated by a linear scheme appropriate for voided materials containing randomly oriented (spheroidal) ellipsoidal voids with the actual void volume-fraction f_e (such as the PCW scheme described in Appendix A). In the case of the fictitious composite with spherical voids, the void volume-fraction f_e is replaced by f_s (which is the equivalent porosity to be determined) and the effective moduli, now denoted by $k^{\hom}_{sph}(f_s)$, $\mu^{\hom}_{sph}(f_s)$, $b_{sph}(f_s)$ and $M_{sph}(f_s)$ for clarity, are estimated by a linear scheme appropriate for voided materials with spherical voids. The identification of the effective elastic moduli in the two composites (with ellipsoidal and spherical voids) leads to the following two equations for a single unknown f_s:

$$k^{\hom}_{\text{ellips}}(f_e, w) = k^{\hom}_{sph}(f_s), \quad \mu^{\hom}_{\text{ellips}}(f_e, w) = \mu^{\hom}_{sph}(f_s). \tag{52}$$

Thanks to (16), the first equality in (52) implies the equality of the two Biot coefficients $b_{\text{ellips}}(f_e, w) = b_{sph}(f_s)$. As for the Biot modulus $1/M$, there remains a small difference in the two moduli $1/M_{\text{ellips}}(f_e, w)$ and $1/M_{sph}(f_s)$ of the order of $(f_e - f_s)/k_0$, which is negligible in the examples that we have in mind (small void volume fraction and quasi-incompressible materials). Therefore, the equality of the two elastic moduli implies, with a very good accuracy, the equality of the four poro-elastic moduli.

Unfortunately, the two equations in Eq. (52) cannot be satisfied by a single porosity f_s. Two "equivalent porosities" must be introduced, f^k_s to meet the first relation in (52) and f^μ_s to meet the second relation

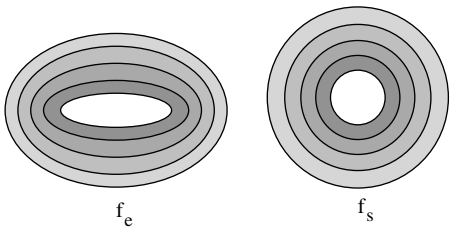

Fig. 10. "Equivalent porosities": the effective elastic properties of the actual configuration (left, porosity f_e) are identical to the effective properties of the virtual configuration with spherical voids (right, porosity f_s).

$$k^{\hom}_{\text{ellips}}(f_e, w) = k^{\hom}_{sph}(f_s^k), \quad \mu^{\hom}_{\text{ellips}}(f_e, w) = \mu^{\hom}_{sph}(f_s^\mu). \tag{53}$$

The effective moduli in the LCC containing ellipsoidal voids can be estimated by the upper bound of Ponte Castañeda and Willis (1995), whereas the effective moduli in the equivalent LCC can be estimated by the Hashin and Shtrikman (1963) upper bound (superscript HS). With these choices, analytical expressions for f_s^k and f_s^μ as functions of f_e and w can be obtained (see Appendix E). To summarize, the mechanical problem for randomly oriented ellipsoidal voids is now translated into a problem for spherical voids which is more amenable to analytical calculations. However, the aspect ratio w of the oblate cavities is not lost in this translation, since f_s^k and f_s^μ both depend on w which remains one of the micromechanical parameters of the model.

A N-phase extension of the model can be proposed for ellipsoidal cavities. First equivalent porosities f_s^k and f_s^μ defined as in (53) are used. Second the effective poro-elastic moduli of the fictitious voided material with spherical voids are now estimated using the N-phase estimate of Hervé and Zaoui (1993) and denoted by k_0^{HZ}, μ_0^{HZ}, b and $1/M$. To be specific, the effective moduli k_0^{HZ}, b and $1/M$ are estimated by the N-phase self-consistent scheme where a sphere containing a central void with porosity f_s^k is subdivided into N different phases. The volume fraction of the ith phase is denoted by f_i^k. Similarly, the effective shear modulus μ_0^{HZ} is estimated by the N-phase self-consistent scheme where a sphere containing a central void with porosity f_s^μ is subdivided into N different phases with volume fraction f_i^μ. The secant moduli and the second moments of the strain-rate field in the phases are obtained by the relations (49) and (51). Finally, the (approximate) N-phase model for randomly distributed ellipsoidal voids in a Gurson matrix can be summarized in the form of the following algorithm:

$$\left.\begin{array}{lcl}
\textit{Initialization} & : & \langle \dot{\varepsilon}_m^2 \rangle_i = \dot{E}_m^2, \quad \langle \dot{\varepsilon}_{\text{eq}}^2 \rangle_i = \dot{E}_{\text{eq}}^2, \quad i = 2, \ldots, N \\
\textit{Iterations} & : & \textit{Do until convergence on } \langle \dot{\varepsilon}_m^2 \rangle_i \textit{ and } \langle \dot{\varepsilon}_{\text{eq}}^2 \rangle_i, \quad i = 2 \ldots N : \\
 & & k_0^{(i)} \textit{ and } \mu_0^{(i)} \textit{ as in } (51) \\
\langle \dot{\varepsilon}_m^2 \rangle_i & = & \dfrac{1}{f_i^k} \dfrac{\partial k_0^{\text{HZ}}(f_s^k)}{\partial k_0^{(i)}} \dot{E}_m^2 + \dfrac{1}{3 f_i^\mu} \dfrac{\partial \mu_0^{\text{HZ}}(f_s^\mu)}{\partial k_0^{(i)}} \dot{E}_{\text{eq}}^2 - \dfrac{2 p^*}{3 f_i^k} \dot{E}_m \dfrac{\partial b(f_s^k)}{\partial k_0^{(i)}} - \dfrac{(p^*)^2}{9 f_i^k} \dfrac{\partial M^{-1}(f_s^k)}{\partial k_0^{(i)}} \\
\langle \dot{\varepsilon}_{\text{eq}}^2 \rangle_i & = & \dfrac{3}{f_i^k} \dfrac{\partial k_0^{\text{HZ}}(f_s^k)}{\partial \mu_0^{(i)}} \dot{E}_m^2 + \dfrac{1}{f_i^\mu} \dfrac{\partial \mu_0^{\text{HZ}}(f_s^\mu)}{\partial \mu_0^{(i)}} \dot{E}_{\text{eq}}^2 - \dfrac{2 p^*}{f_i^k} \dot{E}_m \dfrac{\partial b(f_s^k)}{\partial \mu_0^{(i)}} - \dfrac{(p^*)^2}{3 f_i^k} \dfrac{\partial M^{-1}(f_s^k)}{\partial \mu_0^{(i)}} \\
 & & \textit{Enddo}
\end{array}\right\} \tag{54}$$

As previously, a fixed point algorithm is used to solve this system of equations. The derivatives are computed numerically (by difference quotients). All layers have the same thickness. The final result is clearly an estimate and the accuracy of this estimate is discussed in the next section. Let us just mention that it has been checked in a separate study that this estimate does not violate the two upper bounds (40) and (50).

Once convergence is reached the overall stress $\boldsymbol{\Sigma}$ can be expressed as

$$\boldsymbol{\Sigma} = \Sigma_m \boldsymbol{i} + \frac{2}{3} \Sigma_{\text{eq}} \frac{\dot{\boldsymbol{E}}^{\text{dev}}}{\dot{E}_{\text{eq}}}$$

with

$$\Sigma_m = 3 k_0^{\text{HZ}}(f_s^k) \dot{E}_m - (p_e - p_b)(b(f_s^k) - 1) - p_e, \quad \Sigma_{\text{eq}} = 3 \mu_0^{\text{HZ}}(f_s^\mu) \dot{E}_{\text{eq}}.$$

5.2.2. Comparison with upper bounds, saturated case

Fig. 11 shows that the predictions of the N-phase model does not violate the two upper bounds (40) and (50) at least with the choice of parameters used in this figure. This was confirmed in a separate and more systematic study. Moreover, Figs. 11 and 12 show that, for purely deviatoric loadings, the N-phase estimate with N arbitrary is close to the two-phase estimate

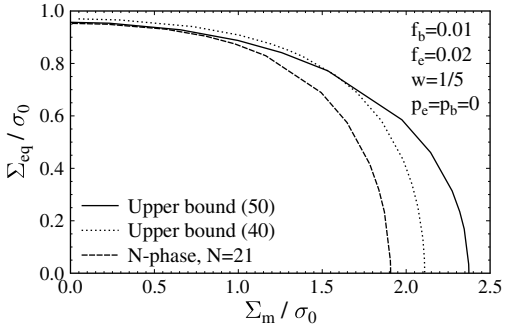

Fig. 11. Gurson matrix containing randomly oriented ellipsoidal voids. $f_e = 0.02$, $f_b = 0.01$, $q_3 = q_1 = 1$, $w = 1/5$. Drained case ($p_b = p_e = 0$). Comparison between different predictions: upper bound (40) (dotted line), upper bound (50) (solid line), N-phase estimate ($N = 21$, dashed line).

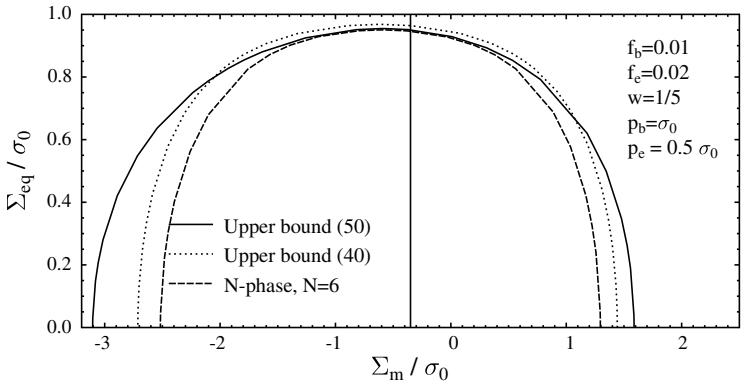

Fig. 12. Gurson matrix containing randomly oriented ellipsoidal voids. $f_e = 0.02$, $f_b = 0.01$, $q_3 = q_1 = 1$, $w = 1/5$. Saturated case $p_b = \sigma_0$, $p_e = \frac{1}{2}\sigma_0$. Comparison between different predictions: upper bound (40) (dotted line), upper bound (50) (solid line), N-phase estimate ($N = 6$, dashed line).

($N = 2$) which coincides with the variational upper bound. Similarly, for a purely hydrostatic loading it is close to the upper bound obtained with the Gurson-like approach (40). Therefore, the N-phase model is close to the best upper bound at all stress triaxialities.

5.2.3. Comparison with finite element calculations, drained case

The use of finite element simulations to assess the accuracy of the estimate (54) for general loading conditions would require full three-dimensional computations performed on a unit-cell containing a large number of randomly oriented ellipsoids. Such calculations are beyond our present computational capabilities. However, when the loading is purely hydrostatic an accurate lower bound can be obtained by means of a simplified unit-cell calculation. Consider as in Fig. 4 an assemblage of self-similar randomly oriented hollow ellipsoids which are identical copies, up to a dilatation and a rotation of a unit pattern Ω. Assume that this volume element V is subjected to a uniform hydrostatic stress Σ_m on its boundary. It is claimed that a lower bound for the limit load for Σ_m can be obtained from the limit load for a *single* hollow ellipsoid to a uniform hydrostatic stress. Indeed the stress field in the single hollow ellipsoid Ω can be continued by a uniform field $\Sigma_m \boldsymbol{i}$ in $V - \Omega$ and the resulting stress field is in equilibrium over V. The procedure can be repeated for all hollow ellipsoids in the assemblage, resulting in a stress field which is in equilibrium in the whole volume element V and which satisfies the yield criterion in each hollow ellipsoid. Therefore, the limit load for a single ellipsoid is a lower bound for the problem posed on the entire volume V. Furthermore, the stress field is the same in each ellipsoid of the assemblage (after dilatation and rotation of the coordinates) since the applied hydrostatic stress is the same in all frames attached to the ellipsoids. All self-similar ellipsoids have the same limit load under hydrostatic stress, no matter their size and orientation. It is therefore sufficient to solve the problem for one single hollow ellipsoid under hydrostatic stress and the corresponding limit load will be a lower bound for the limit load for the whole volume V. The analysis of a single ellipsoid is further simplified by the rotational invariance of the problem and can be reduced to an axisymmetric calculations. Typical meshes used in the FEM analysis of this problem are shown in Fig. 13.

For simplicity, the FEM analysis is performed with a Von Mises matrix ($f_b = 0$) to concentrate the attention on randomly oriented ellipsoidal voids. The estimate of the Section 5.1.1 is carried out with the following coefficients for the LCC:

$$k_0^{(i)} = +\infty \quad \text{and} \quad \mu_0^{(i)} = \frac{\sigma_0}{3\left(\sqrt{\langle \dot{\varepsilon}_{eq}^2 \rangle_i}\right)}. \tag{55}$$

Fig. 14 shows a reasonably good agreement between the FEM results and the model (estimate based on the N-phase model). The FEM simulations are lower bounds to the predictions of the model except when the volume fraction of the large voids becomes very small.

5.2.4. Effect of the two internal pressures on the effective flow surface

When the two populations of voids contain gases with two different pressures p_b and p_e in the small and large voids respectively, the effective flow surface undergoes a change in center and in shape by comparison with that of the drained material with same microstructure (but with $p_b = p_e = 0$). Very little is actually known on these pressures, both on their dependence on the void size and on their scatter. Even their order of magnitude seems to be a subject of debate. Our model allows for a parametric study to be conducted to assess the influence of these pressures.

When the two pressures are identical, $p_b = p_e \neq 0$ it has been shown in Section 4.4 that the effective flow surface of the saturated biporous material is simply obtained from that of the drained material by a shift $-p_e \boldsymbol{i}$ along the hydrostatic axis. The predictions of our model shown in Fig. 15 are consistent with this exact result.

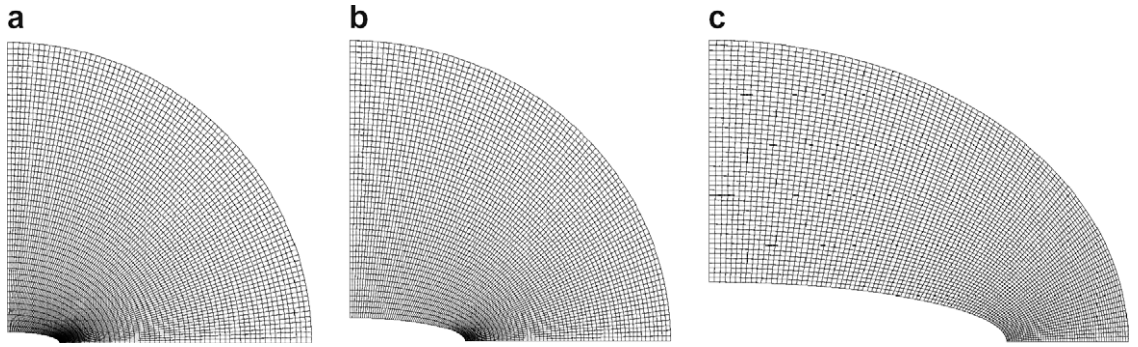

Fig. 13. Meshes used in the unit-cell calculations (a) $f_e = 0.001$, $w = 1/5$, (b) $f_e = 0.01$, $w = 1/5$, (c) $f_e = 0.1$, $w = 1/5$.

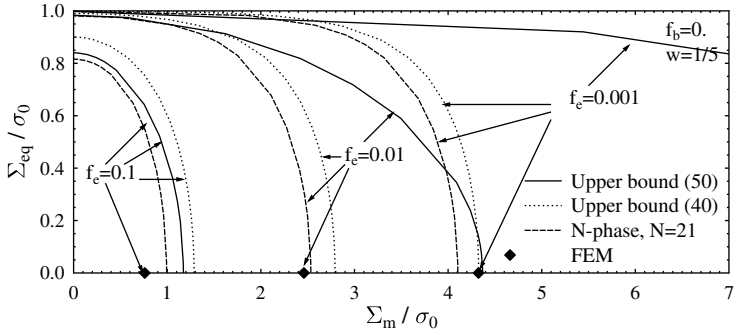

Fig. 14. Randomly oriented ellipsoidal voids ($w = 1/5$) in a von Mises matrix ($f_b = 0$). Drained case ($p_b = p_e = 0$). Comparison between different predictions: upper bound (40) (dotted line), upper bound (50) (solid line), N-phase estimate ($N = 21$, dashed line), FEM simulations (diamond).

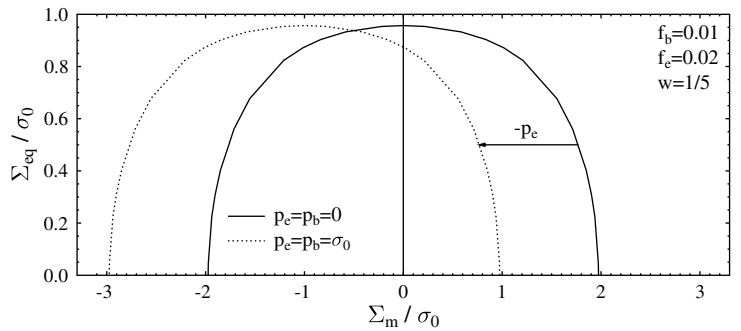

Fig. 15. Gurson matrix containing randomly oriented ellipsoidal voids $f_e = 0.02$, $f_b = 0.01$, $q_3 = q_1 = 1$, $w = 1/5$. Estimate of the effective flow surface based on the N-phase model ($N = 6$). Comparison between the drained case ($p_b = p_e = 0$, dashed line) and the saturated case with $p_b = p_e = \sigma_0$ (solid line).

However, this is no longer the case when the two internal pressures are different. Fig. 16 shows that in addition to a shift along the hydrostatic axis, the effective flow surface undergoes a change in shape and in size. A similar effect has also been observed by Dormieux et al. (2006). In particular the maximal shear (or equivalent stress) which can be sustained by the material is *lowered* by a difference in internal pressures.

6. Conclusion

This study is devoted to a class of porous materials containing two populations of voids subjected to internal pressure. The smallest intragranular voids are spherical in shape whereas the largest, intergranular, pores, are ellipsoidal and randomly oriented. In this first part of the study, attention has been focused on the effective properties of these materials with *fixed* microstructure. Our main findings can be summarized as follows:

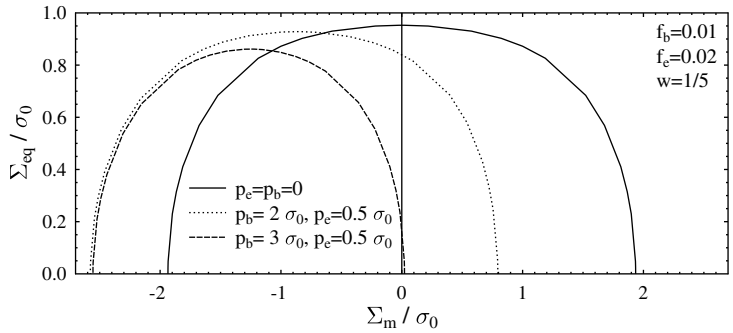

Fig. 16. Gurson matrix containing randomly oriented ellipsoidal voids $f_e = 0.02$, $f_b = 0.01$, $q_3 = q_1 = 1$, $w = 1/5$. N-phase estimate of the effective flow surface ($N = 6$). Comparison between the drained case ($p_b = p_e = 0$, solid line) and two saturated cases $p_b = 2\sigma_0$, $p_e = \frac{1}{2}\sigma_0$ (dotted line) and $p_b = 3\sigma_0$, $p_e = \frac{1}{2}\sigma_0$ (dashed line).

(1) The analysis of Gologanu et al. (1994) devoted to aligned ellipsoidal voids in a von Mises matrix has been extended to randomly oriented ellipsoidal voids in a Gurson matrix. The corresponding result is a rigorous upper bound for the effective flow surface of the biporous material. This bound is sharp under hydrostatic loading.
(2) The variational procedure of Ponte Castañeda (1991) has been applied with a linear comparison composite with only one phase for the matrix. The corresponding result is again an upper bound for the effective flow surface of the biporous material. This bound is sharp under deviatoric loadings.
(3) A N-phase model where the matrix is subdivided in subdomains has been proposed which matches closely the predictions of the two above upper bounds in the range of stress triaxialities where they are separately sharp.
(4) The effect of internal pressures has been discussed. It has been shown that when the two internal pressures coincide, the effective flow surface of the saturated biporous material is obtained from that of the drained material by a shift along the hydrostatic axis. However, when the two pressures are different, the modifications brought to the effective flow surface in the drained case involve not only a translation along the hydrostatic axis but also a change in shape and size of the surface.

Acknowledgements

This work was supported by the grant IRSN-CNRS 31002799 from the French Institut de Radioprotection et de Sûreté Nucléaire and by Electricité de France. This paper was completed during the post-doctoral stay of one of the authors (P.-G.V.) at the Laboratoire de Mécanique et d'Acoustique (CNRS). Fig. 1 (left) is taken from Dubourg et al. (2005), with permission from Elsevier.

Appendix A. Ponte Castañeda and Willis (1995) linear upper bound for porous materials with randomly oriented ellipsoidal voids

Ponte Castañeda and Willis (1995) have derived an upper bound for composite materials composed of a linear-elastic matrix containing linear-elastic inclusions with a (spheroidal) ellipsoidal shape and whose centers are arranged in space according to an ellipsoidal distribution. This bound involves two different $\boldsymbol{P}$ tensors, $\boldsymbol{P}^i$ and $\boldsymbol{P}^d$, corresponding respectively to the shape of the inclusions and to their distribution (see Ponte Castañeda and Willis, 1995 for more details). When specialized to porous materials (matrix with stiffness $\boldsymbol{C}$ containing ellipsoidal voids with porosity f_e) this bound reads as

$$\boldsymbol{C}^{\mathrm{PCW}} = \boldsymbol{C} + f_e\left(\boldsymbol{I} - f_e \oint [(\boldsymbol{P}^i - \boldsymbol{C}^{-1})^{-1}] : \boldsymbol{P}^d\right)^{-1} : \oint [(\boldsymbol{P}^i - \boldsymbol{C}^{-1})^{-1}], \tag{A.1}$$

where the following notations have been used:

(1) $\boldsymbol{I}$ is the fourth-order identity tensor in the vector space of symmetric second-order tensors.
(2) The two $\boldsymbol{P}$ tensors are related to the Eshelby tensors $\boldsymbol{S}^i$ and $\boldsymbol{S}^d$ associated respectively with the ellipsoidal shape and with the ellipsoidal distribution of the voids:

$$\boldsymbol{P}^i = \boldsymbol{S}^i(w) : \boldsymbol{C}^{-1}, \quad \boldsymbol{P}^d = \boldsymbol{S}^d(w^d) : \boldsymbol{C}^{-1},$$

where w and w^d denote the aspect ratio of the inclusions and of the distribution, respectively. Detailed expressions of the Eshelby tensors can be found in Mura (1987).

(3) The symbol $\oint$ denotes the average over all possible orientations. As shown by Gatt et al. (2005), this averaging corresponds to a projection on the fourth-order tensors $\boldsymbol{J}$ and $\boldsymbol{K}$ which extract from any symmetric second-order tensor its hydrostatic part and its deviator:

$$\oint \boldsymbol{C} = P_{JK}(\boldsymbol{C}) = \frac{\boldsymbol{C} :: \boldsymbol{J}}{\boldsymbol{J} :: \boldsymbol{J}}\boldsymbol{J} + \frac{\boldsymbol{C} :: \boldsymbol{K}}{\boldsymbol{K} :: \boldsymbol{K}}\boldsymbol{K}. \tag{A.2}$$

When the void distribution is isotropic ($w^d = 1$, $\boldsymbol{P}^d$ corresponding to spherical symmetry), the bulk and shear moduli k^{PCW} and μ^{PCW} are given by

$$k^{\mathrm{PCW}} = -\frac{k_n}{k_d} \tag{A.3}$$

with

$$\begin{aligned} k_n &= 2k\mu\Big\{k(2f_e + (-3+4f_e)w^2)(-2+w^2+w^4) + 2(-1+f_e)w^2(-1-w^2+2w^4)\mu \\ &\quad + w\arccos(w)\Big[2\sqrt{1-w^2}(3k(1+f_e+(-1+2f_e)w^2) + (-1+f_e)(-1+4w^2)\mu) - .9kw\arccos(w)\Big]\Big\}, \\ k_d &= (-1+w)(1+w)\{3f_e k(1+2w^2)[k(2+w^2)+w^2\mu] + 2w^2\mu[3k(2+w^2)+2\mu+4w^2\mu]\} \\ &\quad + w\arccos(w)\Big\{\sqrt{1-w^2}[9f_e k^2(1+2w^2) + 3k(-4-f_e+4(1+f_e)w^2)\mu + 4(-1+4w^2)\mu^2] + 18kw\mu\arccos(w)\Big\}. \end{aligned} \tag{A.4}$$

The analytical expression of μ^{PCW} is too complicated to be given here. Since we are interested in rather flat intergranular voids, a Taylor expansion at first order in w (for w small) can be performed. It should be noted that, for small w, f_e is of the same order as w. A change of variable can be done setting $f_e = \alpha_c w$ with

$$\alpha_c = \frac{4}{3}\frac{\pi(b_1)^3 N_c}{|V|}, \tag{A.5}$$

where N_c denotes the number of cavities contained in V and b_1 is the long semi-axe of the ellipsoidal void (see Appendix B). Then the Taylor expansion of μ^{PCW} at first-order in w reads as

$$\begin{aligned} \mu^{\mathrm{PCW}} &= (\mu(5625\pi^2 w^2(3k+\mu)^2(3k+2\mu)^2 - 96f_e^2(k+2\mu)(9k+4\mu)^2(9k+8\mu) + 25f_e w(-81k^4(800w + 9\pi(4 \\ &\quad + 15\pi w)) - 108k^3(3\pi + 5(304+45\pi^2)w)\mu - 54k^2(-68\pi + 5(496+69\pi^2)w)\mu^2 - 24k(-96\pi + 5(368 \\ &\quad + 45\pi^2)w)\mu^3 - 8(-48\pi + 640w + 45\pi^2 w)\mu^4)))/(9(25\pi w(3k+\mu)(3k+2\mu) + 8f_e(k+2\mu)(9k+4\mu))^2) \\ &\quad + o(w) \end{aligned} \tag{A.6}$$

Remark. The prediction (A.1) is an upper bound for the actual effective stiffness of the composite as long as $f_e \leqslant w$.

Appendix B. Hollow ellipsoids

The inner and the outer boundary of the reference volume are two confocal spheroids (ellipsoids which are rotation invariant around the z axis). Denoting as in Fig. 17 by a_1 and b_1 the horizontal and the vertical semi-axes of the inner spheroid (similar notation for the outer spheroid with index 2), the void volume-fraction and the void aspect-ratio can be expressed as

$$f_e = \frac{a_1 b_1^2}{a_2 b_2^2} \ \text{(volume fraction)}, \quad w = \frac{a_1}{b_1} \ \text{(aspect ratio)}.$$

Since the inner and the outer ellipsoids are confocal, their focii are located on a circle of radius c given by

$$c = \sqrt{b_1^2 - a_1^2} = \sqrt{b_2^2 - a_2^2}.$$

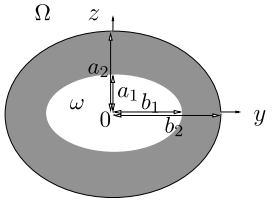

Fig. 17. Notations for the hollow spheroid of reference.

A family of confocal ellipsoids with horizontal axis a and vertical axis b, parameterized by a scalar λ, is introduced through the following relations:

$$a = c\ \sinh\lambda, \quad b = c\ \cosh\lambda,$$

where λ varies between λ_1 and λ_2:

$$a_1 = c\ \sinh\lambda_1, \quad b_1 = c\ \cosh\lambda_1, \quad a_2 = c\ \sinh\lambda_2, \quad b_2 = c\ \cosh\lambda_2.$$

Then, one defines

$$R(\lambda) = -\frac{ac}{b^2} + \mathrm{Arcsin}\left(\frac{c}{b}\right), \quad Z(\lambda) = \frac{2c}{a} - 2\mathrm{Arcsin}\left(\frac{c}{b}\right), \quad R_2 = R(\lambda_2), \quad Z_2 = Z(\lambda_2), \mid \Omega \mid = \frac{4}{3}\pi a_2 b_2^2,$$
$$\tilde{\alpha} = \frac{a_2 b_2^2}{2c^3}, \quad J(\lambda) = \frac{4}{3}\frac{\pi b(2a^2 + b^2)}{\mid \Omega \mid}, \tag{B.1}$$

$$Q_J(\lambda) = \frac{4}{9}\frac{b\pi}{\mid \Omega \mid}\{b^2[-1 + 6R(\lambda)\tilde{\alpha} + 3Z_2\tilde{\alpha}]^2 + 2a^2[1 - 6Z_2\tilde{\alpha} + 12R^2(\lambda)\tilde{\alpha}^2 + 12Z^2(\lambda)\tilde{\alpha}^2 + 9Z_2^2\tilde{\alpha}^2 + 6Z(\lambda)\tilde{\alpha}(1 + 2R(\lambda)\tilde{\alpha} - 3Z_2\tilde{\alpha})]\}. \tag{B.2}$$

Appendix C. Generalized *N*-phase self-consistent scheme

C.1. Linear elastic effective properties

Hervé and Zaoui (1993) have proposed a generalized N-phase self-consistent scheme where a spherical inclusion is surrounded by $N-1$ concentric spherical shells (see Fig. 6 left). The outer infinite medium, indexed by $N+1$, is subjected to an applied strain $\boldsymbol{E}$ at infinity. All phases are linear elastic and isotropic. The overall bulk and shear overall moduli are determined in a self consistent way, but assigning to the outer medium the (unknown) effective properties of the composite. This scheme can be applied to the problem of a central void surrounded by $N-1$ spherical elastic layers. The effective elastic properties of the composite and the strain localization tensors $\boldsymbol{A}^{(i)}$ can be explicitly expressed in terms of the elastic moduli of the individual constituents and of the volume fraction of the phases. The reader is referred to Hervé and Zaoui (1993) for full details, we limit ourself here to the derivation of the effective bulk modulus which turns out to be very similar to the derivation of the effective Biot tensor and Biot modulus. The following notations will be used: the central void is phase 1 ($i=1$), R_i denotes the external radius of the i-th layer, $1 \leqslant i \leqslant N$, R_N is arbitrary, so that it can chosen equal to 1. Consequently, $f = c^{(1)} = R_1^3$. The moduli of the ith phase ($1 \leqslant i \leqslant N$) are denoted by $k_0^{(i)}$ and $\mu_0^{(i)}$.

In a first stage, the part of the localization tensor $\boldsymbol{A}^{(1)}$ corresponding to hydrostatic deformation is determined by subjecting the infinite medium depicted in Fig. 6 right to a hydrostatic deformation $\boldsymbol{i}$ at infinity, the void being stress-free. In view of the spherical symmetry of the problem, the displacement is radial in each spherical shell, $\boldsymbol{u} = u_r(r)\ \boldsymbol{e}_r$ where u_r is classically (in linear, isotropic elasticity) in the form $u_r = A_i r + B_i/r^2$. The unknowns (A_i, B_i) in each layer solve an algebraic system obtained by requiring continuity of the radial displacement and of the traction across the interface between the layers, by imposing an internal pressure $p=1$ in the void and a linear displacement at infinity.

$$A_i R_i + \frac{B_i}{R_i^2} = A_{i+1}R_i + \frac{B_{i+1}}{R_i^2}, \quad 2 \leqslant i \leqslant N, \tag{C.1}$$

$$3k_0^{(i)}A_i - \frac{4\mu_0^{(i)}B_i}{R_i^3} = 3k_0^{(i+1)}A_{i+1} - \frac{4\mu_0^{(i+1)}B_{i+1}}{R_i^3}, \quad 2 \leqslant i \leqslant N, \tag{C.2}$$

$$3k_0^{(2)}A_2 - \frac{4\mu_0^{(2)}B_2}{R_1^3} = -p, \tag{C.3}$$

$$3k_0^{(N)}A_N - \frac{4\mu_0^{(N)}B_N}{R_N^3} = 3k_0^{HZ}A_{N+1} - \frac{4\mu_0^{HZ}B_{N+1}}{R_N^3} - b_0^{HZ}p, \tag{C.4}$$

$$A_{N+1} = E_m, \tag{C.5}$$

where k_0^{HZ} μ_0^{HZ} and b_0^{HZ} are unknown and where in the purely elastic case (drained case) considered in this subsection $p=0$ and $E_m = 1$. The continuity relations in the solid phase (C.1) and (C.2) can be rewritten as

$$\boldsymbol{J}_i(R_i)\boldsymbol{M}_i = \boldsymbol{J}_{i+1}(R_i)\boldsymbol{M}_{i+1}, \quad \text{with } \boldsymbol{M}_i = \begin{pmatrix} A_i \\ B_i \end{pmatrix}, \qquad \boldsymbol{J}_i(r) = \begin{pmatrix} r, & \frac{1}{r^2} \\ 3k_0^{(i)}, & \frac{-4\mu_0^{(i)}}{r^3} \end{pmatrix}. \tag{C.6}$$

Therefore, the unknowns $\boldsymbol{M}_i,\ 2 \leqslant i \leqslant N$ are related by

$$\boldsymbol{M}_{i+1} = \boldsymbol{H}_i \boldsymbol{M}_2, \quad \boldsymbol{H}_i = \boldsymbol{N}_i \cdot \ldots \cdot \boldsymbol{N}_2, \quad \boldsymbol{N}_i = \boldsymbol{J}_{i+1}(R_i)^{-1} \boldsymbol{J}_i(R_i).$$

Similarly, the three remaining relations can be written as (with $R_1^3 = f$)

$$\boldsymbol{J}_N(R_N) \cdot \boldsymbol{H}_{N-1} \cdot \begin{pmatrix} \frac{4\mu_0^{(2)} B_2}{3fk_0^{(2)}} \\ B_2 \end{pmatrix} = \boldsymbol{J}_{N+1}(R_N) \cdot \begin{pmatrix} 1 \\ B_{N+1} \end{pmatrix}. \tag{C.7}$$

The above relations give two equations for the four unknowns B_2, B_{N+1} and k_0^{HZ} and μ_0^{HZ} (which enter the definition of $\boldsymbol{J}_{N+1}(R_N)$). The missing equations are given by the self consistent condition. Hervé and Zaoui (1993) have shown that the condition of self-consistency is equivalent to imposing that the average strain in the first N layers (sphere of radius R_N) coincides with the strain at infinity. In the present situation self-consistency implies $\langle \varepsilon_m \rangle = E_m = 1$, or equivalently:

$$\frac{1}{\frac{4}{3}\pi R_N^3} \int_{r=R_N} \boldsymbol{u} \cdot \boldsymbol{n}\, \mathrm{d}s = 3E_m = 3. \tag{C.8}$$

Taking into account the form of $\boldsymbol{u}$ and the fact that $R_N = 1$ and $A_{N+1} = 1$, the above relation gives that $B_{N+1} = 0$. Defining $\boldsymbol{L} = \boldsymbol{J}_N(R_N) \cdot \boldsymbol{H}_{N-1}$ the solution of (C.7) reads as

$$B_2 = \frac{1}{L_{11} \frac{4\mu_0^{(2)}}{3fk_0^{(2)}} + L_{12}}.$$

Finally the effective bulk modulus can be deduced from the relation (C.4)

$$3k_0^{HZ} = \frac{L_{21} \frac{4\mu_0^{(2)}}{3fk_0^{(2)}} + L_{22}}{L_{11} \frac{4\mu_0^{(2)}}{3fk_0^{(2)}} + L_{12}}.$$

The expression of the effective shear modulus μ_0^{HZ} can be found in Hervé and Zaoui (1993).

It should be noted for further use in the computation of the Biot tensor that the localization tensor $\boldsymbol{A}^{(1)}$ in phase 1 satisfies

$$\boldsymbol{i} : \boldsymbol{A}^{(1)} = A_1 \boldsymbol{i}, \quad A_1 = A_2 + \frac{B_2}{R_1^3} = \frac{3k_0^{(2)} + 4\mu_0^{(2)}}{3fk_0^{(2)} \left(L_{11} \frac{4\mu_0^{(2)}}{3fk_0^{(2)}} + L_{12} \right)}.$$

C.2. Linear poro-elastic phases

The N-phase self-consistent scheme can be extended to linear poro-elastic phases. The Biot tensor $\boldsymbol{B}$ is given by the first relation in (13):

$$\boldsymbol{B} = b_0^{\mathrm{HZ}} \boldsymbol{i}, \quad b_0^{\mathrm{HZ}} = \frac{3k_0^{(2)} + 4\mu_0^{(2)}}{3k_0^{(2)} \left(L_{11} \frac{4\mu_0^{(2)}}{3fk_0^{(2)}} + L_{12} \right)}. \tag{C.9}$$

The evaluation of the Biot modulus M requires the evaluation of $\boldsymbol{i} : \boldsymbol{a}^{(1)}$ which is the change in volume of the void when it is subjected to an internal unit pressure with zero displacement at infinity. Due to the spherical symmetry of the problem, the displacement is radial with the same form as in the previous subsection with two unknowns (A_i, B_i) in phase i. These unknowns solve the system (C.1), (C.2), (C.3), (C.4), (C.5) where now $E_m = 0$ and $p \neq 0$ and finally one obtains the following two equations, for the three unknowns B_2, B_{N+1} and b_0^{hom} (b_0^{hom} is considered as unknown at this stage but it will be checked that its final expression coincides with (C.9)):

$$\boldsymbol{J}_N(R_N) \cdot \boldsymbol{H}_{N-1} \cdot \begin{pmatrix} \frac{-p}{3k_0^{(2)}} + \frac{4\mu_0^{(2)} B_2}{3R_1^3 k_0^{(2)}} \\ B_2 \end{pmatrix} = \boldsymbol{J}_{N+1}(R_N) \cdot \begin{pmatrix} 0 \\ B_{N+1} \end{pmatrix} + \begin{pmatrix} 0 \\ -b_0^{HZ} p \end{pmatrix}. \tag{C.10}$$

The self-consistency condition implies $B_{N+1} = 0$. Finally,

$$B_2 = \frac{L_{11} p}{3k_0^{(2)} \left(L_{11} \frac{4\mu_0^{(2)}}{3fk_0^{(2)}} + L_{12} \right)}, \quad b_0^{\mathrm{hom}} = \frac{L_{21} L_{12} - L_{11} L_{22}}{3k_0^{(2)} \left(L_{11} \frac{4\mu_0^{(2)}}{3fk_0^{(2)}} + L_{12} \right)}. \tag{C.11}$$

For consistency, the expression of b_0^{HZ} given in (C.11) should coincide with that given in (C.9). This is a consequence of the following relations:

$$\det(\boldsymbol{J}_i(r)) = -\frac{3k_0^{(i)}+4\mu_0^{(i)}}{r^2}, \quad \det(\boldsymbol{N}_i) = \frac{3k_0^{(i)}+4\mu_0^{(i)}}{3k_0^{(i+1)}+4\mu_0^{(i+1)}},$$

$$\det(\boldsymbol{H}_{N-1}) = \frac{3k_0^{(2)}+4\mu_0^{(2)}}{3k_0^{(N)}+4\mu_0^{(N)}}, \quad L_{21}L_{12}-L_{11}L_{22} = -\det(\boldsymbol{L}) = (3k_0^{(2)}+4\mu_0^{(2)}).$$

Finally,

$$\boldsymbol{a}^{(1)} = A_1\boldsymbol{i}, \quad A_1 = A_2 + \frac{B_2}{R_1^3} = -\frac{p}{3k_0^{(2)}} + \frac{3k_0^{(2)}+4\mu_0^{(2)}}{3fk_0^{(2)}} \frac{L_{11}p}{\left(L_{11}\frac{4\mu_0^{(2)}}{3fk_0^{(2)}}+L_{12}\right)} \frac{1}{3k_0^{(2)}}$$

and

$$\frac{1}{M} = -\frac{f}{k_0^{(2)}} + \frac{3k_0^{(2)}+4\mu_0^{(2)}}{k_0^{(2)}} \frac{L_{11}}{\left(L_{11}\frac{4\mu_0^{(2)}}{3fk_0^{(2)}}+L_{12}\right)} \frac{1}{3k_0^{(2)}}.$$

Appendix D. Hollow sphere made of a Gurson material under hydrostatic loading and internal pressure

The problem of a hollow sphere Ω made of a Gurson matrix, containing a *stress-free* central void (i.e. $\boldsymbol{\sigma}\cdot\boldsymbol{n} = \boldsymbol{0}$ on the inner boundary of Ω) and subjected to hydrostatic tension $\boldsymbol{\sigma}\cdot\boldsymbol{n} = \Sigma_m\boldsymbol{n}$ on its outer boundary has been solved by Perrin (1992). An extension of this problem to the saturated case is proposed here. A hollow sphere Ω made of a Gurson matrix with pressure p_b, contains a central void with pressure p_e and is subjected to hydrostatic stress. By the change of variable $\boldsymbol{\sigma}^* = \boldsymbol{\sigma} + p_b\boldsymbol{i}$, the boundary conditions read as

$$\frac{\sigma_{rr}^*}{\sigma_0}(r=a) = \frac{p_b-p_e}{\Sigma_0}, \quad \frac{\sigma_{rr}^*}{\sigma_0}(r=b) = \frac{\Sigma_m}{\sigma_0}+\frac{p_b}{\sigma_0},$$

where a and b denote the inner and outer radii of the hollow sphere. Using the same change of variables as Perrin (1992), $u(r) = \sigma_{rr}^*/\sigma_0$ and $v(r) = (\sigma_{\theta\theta}^* - \sigma_{rr}^*)/\sigma_0$, the yield function in the matrix can be rewritten as

$$v^2 + 2f_b\cosh\left(\frac{3}{2}u+v\right) - 1 - f_b^2 = 0. \tag{D.1}$$

The boundary conditions and the radial equilibrium read as

$$u(a) = \frac{p_b-p_e}{\sigma_0}, \quad u(b) = \frac{\Sigma_m}{\sigma_0}+\frac{p_b}{\sigma_0}, \quad \frac{\mathrm{d}u}{\mathrm{d}r} = \frac{2v}{r}. \tag{D.2}$$

Assuming that the matrix is everywhere in the plastic regime, the yield condition (D.1) can be differentiated to obtain

$$2v\,\mathrm{d}v + 2f_b\left(\frac{3}{2}\mathrm{d}u + \mathrm{d}v\right)\sinh\left(\frac{3}{2}u+v\right) = 0. \tag{D.3}$$

It follows from the equation of radial equilibrium that $du = \frac{2v}{r}dr$ and from the yield condition (D.1) that $\sinh\left(\frac{3}{2}u+v\right) = \pm\sqrt{(1+f_b^2-v^2)^2-4f_b^2}/(2f_b)$. The sign $\pm$ is the sign of the hydrostatic stress $\left(\frac{3}{2}u+v\right)$ in the matrix. This sign is assumed to be the same throughout the matrix. Finally (D.3) writes

$$\frac{3\,\mathrm{d}r}{r} = \mp\frac{2\,\mathrm{d}v}{\sqrt{(1+f_b^2-v^2)^2-4f_b^2}} - \frac{\mathrm{d}v}{v}, \tag{D.4}$$

which gives by integration between the inner and outer radii

$$\frac{b^3}{a^3}\frac{v(b)}{v(a)} = \exp\left(\mp 2\int_{v(a)}^{v(b)} \frac{\mathrm{d}v}{\sqrt{(1+f_b^2-v^2)^2-4f_b^2}}\right). \tag{D.5}$$

The boundary condition and the yield criterion at $r=a$ give

$$v^2(a) + 2f_b\cosh\left(\frac{3}{2}\frac{p_b-p_e}{\sigma_0}+v(a)\right) - 1 - f_b^2 = 0. \tag{D.6}$$

Similarly, the boundary conditions and the yield criterion at $r=b$ gives

$$\frac{\Sigma_m}{\sigma_0} = -\frac{p_b}{\sigma_0} + \frac{2}{3}\left(\pm\operatorname{arccosh}\left(\frac{1+f_b^2-v^2(b)}{2f_b}\right) - v(b)\right). \tag{D.7}$$

The sign $\pm$ in (D.7) is opposite to the undetermined sign in Eq. (D.5). The indeterminacy is resolved in the following way. First Eq. (D.6) is solved and has two possible roots $v(a)$. Then (D.5) is solved with these two values for $v(a)$, this gives four possible values for $v(b)$ which, when incorporated in Eq. (D.7), give four values for the hydrostatic stress Σ_m. Only two of them are consistent with the assumption that $\frac{3}{2}u+v$ does not change sign in the matrix. The two admissible roots give the two purely hydrostatic points on the yield surface. One of them is such that $\frac{3}{2}u(b)+v(b)$ and $\frac{3}{2}u(a)+v(a)$ are both positive and $v(b)$ is solution of (D.5) with $\pm=+$. The other one is such that $\frac{3}{2}u(b)+v(b)$ and $\frac{3}{2}u(a)+v(a)$ are both negative and $v(b)$ is solution of (D.5) with $\pm=-$.

Appendix E. Equivalent porosities

When the Ponte Castañeda and Willis (1995) and the Hashin and Shtrikman (1963) upper bounds are chosen to estimate the linear effective moduli of the composite with ellipsoidal voids and of the composite with spherical voids, the two equivalent porosities f_s^k and f_s^μ solve the two equations

$$k_0^{\mathrm{PCW}}(f_e)=k_0^{\mathrm{HS}}(f_s^k),\quad \mu_0^{\mathrm{PCW}}(f_e)=\mu_0^{\mathrm{HS}}(f_s^\mu). \tag{E.1}$$

These equivalent porosities depend not only on f_e but also on the void aspect-ratio w and on the moduli of the matrix k_0 and μ_0. The matrix being almost incompressible (at least for small f_b which is the case in the practical applications which we have in mind), an additional approximation is introduced by considering k_0 to be infinite. Under this approximation, the equivalent porosities f_s^k and f_s^μ depend only on f_e and w and write

$$f_s^k=\frac{2f_e(1+2w^2)[-2+w^2+w^4+3w\sqrt{1-w^2}\arccos(w)]}{3w[-2w+w^3+w^5-2(1-w^2)^{3/2}\arccos(w)+3w(\arccos(w))^2]},\quad f_s^\mu=\frac{f_{sn}^\mu}{f_{sd}^\mu} \tag{E.2}$$

with

$$\begin{aligned}f_{sn}^\mu=&\,4f_e(-1+w^2)^2[w(-1+w^2)^2(-4-65w^2-44w^4+14w^6)-3\sqrt{1-w^2}(-12+40w^2-83w^4\\&+55w^6)\arccos(w)+9w(-3+21w^2-26w^4+8w^6)(\arccos(w))^2-27w^2\sqrt{1-w^2}(1+2w^2)(\arccos(w))^3],\end{aligned} \tag{E.3}$$

$$\begin{aligned}f_{sd}^\mu=&\,25w[w^2(-1+w^2)^2(-56+22w^2-9w^4-13w^6+2w^8)-2w\sqrt{1-w^2}(16-99w^2+119w^4-58w^6\\&+21w^8+w^{10})\arccos(w)+6(-1+w^2)^2(4+19w^2-8w^4+3w^6)(\arccos(w))^2-18w\sqrt{1-w^2}(3+4w^2\\&-2w^4+w^6)(\arccos(w))^3+27(w^2+w^4)(\arccos(w))^4].\end{aligned} \tag{E.4}$$

References

Benzerga, A., 2002. Micromechanics of coalescence in ductile fracture. J. Mech. Phys. Solids 50, 1331–1362.

Bilger, N., Auslender, F., Bornert, M., Masson, R., 2002. New bounds and estimates for porous media with rigid perfectly plastic matrix. Comptes Rendus Mécanique 330, 127–132.

Buryachenko, V., 1996. The overall elastoplastic behavior of multiphase materials with isotropic components. Acta Mech. 119, 93–117.

Canon, R., Roberts, J., Beals, R., 1971. Deformation of UO_2 at high temperatures. J. Am. Ceram. Soc. 54 (2), 105–112.

Dherbey, F., Louchet, F., Mocellin, A., Leclercq, S., 2002. Elevated temperature creep of polycrystalline uranium dioxide: from microscopic mechanisms to macroscopic behaviour. Acta Mater. 50, 1495–1505.

Dormieux, L., Kondo, D., Ulm, F., 2006. Microporomechanics. Wiley, UK.

Dormieux, L., Molinari, A., Kondo, D., 2002. Micromechanical approach to the behavior of poroelastic materials. J. Mech. Phys. Solids 50, 2203–2231.

Dubourg, R., Faure-Geors, H., Nicaise, G., Barrachin, M., 2005. Fission product release in the first two PHEBUS tests FPT0 and FPT1. Nucl. Eng. Design 235, 2183–2208.

Fabrègue, D., Pardoen, T., 2008. A constitutive model for elastoplastic solids containing primary and secondary voids. J. Mech. Phys. Solids 56, 719–741.

Gatt, J., Monerie, Y., Laux, D., Baron, D., 2005. Elastic behavior of porous ceramics: application to nuclear fuel materials. J. Nucl. Mater. 336, 145–155.

Gologanu, M., Leblond, J.B., Devaux, J., 1993. Approximate models for ductile metals containing non-spherical voids-case of axisymmetric prolate ellipsoidal cavities. J. Mech. Phys. Solids 41, 1723–1754.

Gologanu, M., Leblond, J.B., Devaux, J., 1994. Approximate models for ductile metals containing non-spherical voids-case of axisymmetric oblate ellipsoidal cavities. ASME J. Eng. Mater. Technol. 116, 290–297.

Gărăjeu, M., Suquet, P., 1997. Effective properties of porous ideally plastic or viscoplastic materials containing rigid particles. J. Mech. Phys. Solids 45, 873–902.

Guerin, Y., 1975. Etude par compression à hautes températures de la déformation plastique du bioxyde d'uranium polycristallin. J. Nucl. Mater. 56, 61–75.

Gurson, A., 1977. Continuum theory of ductile rupture by void nucleation and growth: Part I – yield criteria and flow rules for porous ductile media. J. Eng. Mater. Technol. 99, 1–15.

Hashin, Z., Shtrikman, S., 1963. A variational approach to the theory of the elastic behavior of multiphase materials. J. Mech. Phys. Solids 11, 127–140.

Hervé, E., Zaoui, A., 1993. N-layered inclusions-based micromechanical modelling. Int. J. Eng. Sci. 31 (1), 1–10.

Hu, G., 1996. A method of plasticity for general aligned spheroidal void or fiber-reinforced composites. Int. J. Plasticity 12, 439–449.

Kashibe, S., Une, K., 1991. Effects of temperature cycling and heating rate on fission gas release of bwr fuels. J. Nucl. Sci. Technol. 28, 1090–1099.

Kashibe, S., Une, K., Nogita, K., 1993. Formation and growth of intragranular fission gas bubbles in UO_2 fuels with burnup of 6–83 GWd/t. J. Nucl. Mater. 206, 22–34.

Koplik, J., Needleman, A., 1988. Void growth and coalescence in porous plastic solids. Int. J. Solids Struct. 24, 835–853.

Kreher, W., Pompe, W., 1985. Field fluctuations in a heterogeneous elastic material – an information theory approach. J. Mech. Phys. Solids 33, 419–445.

Leblond, J.B., 2002. Mécanique de la Rupture fragile et ductile. Hermès, Paris.

Leblond, J.B., Perrin, G., Suquet, P., 1994. Exact results and approximate models for porous viscoplastic solids. Int. J. Plasticity 10, 213–235.

Lösönen, P., 2000. On the behaviour of intragranular fission gas in UO_2 fuel. J. Nucl. Mater. 280, 56–72.

Marini, B., Mudry, F., Pineau, A., 1985. Experimental study of cavity growth in ductile rupture. Eng. Fract. Mech. 22, 989–996.
Martin, D., 1989. The elastic constants of polycrystalline UO_2 and U,PU mixed oxides: a review and recommendations. High Temperatures-High Pressures 21, 13–24.
Michel, J., Moulinec, H., Suquet, P., 1999. Effective properties of composite materials with periodic microstructure: a computational approach. Comp. Meth. Appl. Mech. Eng. 172, 109–143.
Monerie, Y., Gatt, J.M., 2006. Overall viscoplastic behavior of non-irradiated porous nuclear ceramics. Mech. Mater. 38, 608–619.
Mura, T., 1987. Micromechanics of Defects in Solids. Martinus Nijhoff, Dordrecht.
Olander, D., 1976. Fundamental Aspects of Nuclear Reactor Fuel Elements. Technical Information Center, U.S. Department of Energy.
Pardoen, T., Hutchinson, J., 2000. An extended model for void growth and coalescence. J. Mech. Phys. Solids 48, 2467–2512.
Perrin, G., 1992. Contribution à l'étude théorique et numérique de la rupture ductile des métaux. Ph.D. thesis, Ecole Polytechnique, Paris.
Perrin, G., Leblond, J.B., 1990. Analytical study of a hollow sphere made of plastic porous material and subjected to hydrostatic tension. Application to some problems in ductile fracture of metals. Int. J. Plasticity 6, 677–699.
Ponte Castañeda, P., 1991. The effective mechanical properties of nonlinear isotropic composites. J. Mech. Phys. Solids 39, 45–71.
Ponte Castañeda, P., Suquet, P., 1998. Nonlinear composites. Adv. Appl. Mech. 34, 171–302.
Ponte Castañeda, P., Willis, J., 1995. The effect of spatial distribution on the effective behaviour of composite materials and cracked media. J. Mech. Phys. Solids 43, 1919–1951.
Ponte Castañeda, P., Zaidman, M., 1996. The finite deformation of nonlinear composite materials. I. Instantaneous constitutive relations. Int. J. Solids Struct. 33, 1271–1286.
Qiu, Y., Weng, G., 1992. A theory of plasticity for porous materials and particle-reinforced composites. J. Appl. Mech. 59, 261–268.
Sauter, F., Leclercq, S., 2003. Modeling of the non-monotonous viscoplastic behavior of uranium dioxide. J. Nucl. Mater. 322, 1–14.
Suquet, P., 1987. Elements of Homogenization for Inelastic Solid Mechanics. In: Sanchez-Palencia, E., Zaoui, A. (Eds.), Homogenization Techniques for Composite Media. Vol. 272 of Lecture Notes in Physics. Springer, New York, pp. 193–278.
Suquet, P., 1995. Overall properties of nonlinear composites: a modified secant moduli theory and its link with Ponte Castañeda's nonlinear variational procedure. C. R. Acad. Sci. Paris 320 (Série IIb), 563–571.
Tvergaard, V., 1990. Material failure by void growth to coalescence. In: Hutchinson, J., Wu, T. (Eds.), Advances in Applied Mechanics, vol. 27. Academic Press, New York, pp. 83–151.
Tvergaard, V., 1998. Interaction of very small voids with larger voids. Int. J. Solids Struct. 35, 3989–4000.
Vincent, P.G., Monerie, Y., Suquet, P., 2008. Ductile damage of porous materials with two populations of voids. C. R. Mecanique 336, 245–259.
Willis, J., 1981. Variational and related methods for the overall properties of composites. In: Yih, C. (Ed.), Advances in Applied Mechanics, vol. 21. Academic Press, New York, pp. 1–78.
Zaidman, M., Ponte Castañeda, P., 1996. The finite deformation of nonlinear composite materials II Evolution of the microstructure. Int. J. Solids Struct. 33, 1287–1303.